MEMS-Based Micro Gas Chromatography: Design, Fabrication and Characterization

Mohammad Amin Zareian-Jahromi

Thesis submitted to the faculty of the
Virginia Polytechnic Institute and State University
in partial fulfillment of the requirements for the degree of

Master of Science
In
Electrical and Computer Engineering

Masoud Agah (chair)
Guo Quan Lu
Kathleen Meehan
Sanjay Raman

May 22, 2009
Blacksburg, VA

Keywords: MEMS, μGC, Multicapillary Separation Column, Stationary Phase, Monolayer Protected Gold

MEMS-Based Micro Gas Chromatography: Design, Fabrication and Characterization

Mohammad Amin Zareian-Jahromi

(ABSTRACT)

This work is focused on the design, fabrication and characterization of high performance MEMS-based micro gas chromatography columns having wide range of applications in the pharmaceutical industry, environmental monitoring, petroleum distillation, clinical chemistry, and food processing. The first part of this work describes different approaches to achieve high-performance microfabricated silicon-glass separation columns for micro gas chromatographic (μGC) systems. The capillary width effect on the separation performance has been studied by characterization of 250 μm-, 125 μm-, 50 μm-, and 25 μm-wide single-capillary columns (SCCs) fabricated on a 10×8 mm^2 die. The plate number of 12500/m has been achieved by 25 μm-wide columns coated by a thin layer of polydimethylsiloxane stationary phase using static coating technique. To address the low sample capacity of these narrow columns, this work presents the first generation of MEMS-based "multicapillary" columns (MCCs) consisting of a bundle of narrow-width rectangular capillaries working in parallel. The second contribution of this work is the first MEMS-based stationary phase coating technique called monolayer protected gold (MPG) for ultra-narrow single capillary (SCC) and multicapillary (MCC) microfabricated gas chromatography (μGC) columns yielding the highest separation performance reported to date. This new μGC stationary phase has been achieved by electrodepositing a uniform functionalized gold layer with an adjustable thickness (250nm-2μm) in 25μm-wide single columns as well as in four-capillary MCCs. The separation performance, stability, reproducibility and bleeding of the stationary phase have been evaluated over time by separating n-alkanes as non-polar and alcohols as polar gas mixtures.

In the name of god

Contents

List of Figures

List of Tables

Grant Information

This work has been supported primarily by the National Science Foundation under Award Number ECCS-0601456.

Dedication

This thesis is dedicated to my wonderful parents, Hajagha and Saadat, who have raised me to be the person I am today. You have been with me every step of the way, through good times and bad. Thank you for all the unconditional love, guidance, and support that you have always given me, helping me to succeed and instilling in me the confidence that I am capable of doing anything I put my mind to.

Thank you for everything.

I am proud of you.

I love you.

Acknowledgments

I would like to formally thank:

- ✓ Dr. Masoud Agah, my advisor, for his hard work and guidance throughout this entire thesis process and for believing in my abilities. I have learned so much, and without you, this would not have been possible. Thank you so much for a great experience and wonderful opportunities. I dedicate all of my future achievements to you because you taught me how to think, how to find a way and how to present my work.
- ✓ Dr. Kathleen Meehan, for serving on my thesis committee. Thank you for your great ideas and guidance throughout this project.
- ✓ Dr. Guo Quan Lu, for serving on my thesis committee.
- ✓ Dr. Sanjay Raman, for serving on my thesis committee.
- ✓ Dr. Mehdi Ashraf-Khorasani, for friendship and technical support.
- ✓ My parents, for their never-ending love and support in all my efforts. Thank you, Mom and Dad.
- ✓ My brother, Hamid, for his love and support throughout the years.
- ✓ My friends and coworkers, Mehdi and Bassam, for friendship and support throughout last three years in our tiny Blacksburg. Thank you for all the memorial moments in VT MEMS Lab.
- ✓ My roommates, Ali and Amin, for the laughing and the fighting, and everything in between.
- ✓ My friend, Diane, for friendship and support.

1 Introduction

1.1 Gas Chromatography

Gas Chromatography (GC) is one of the most widely applied methods of identification in analytical chemistry. This physical method of in-time separation of volatile and semi-volatile gaseous mixtures was introduced in 1950s. As an analytical tool, GC has a wide range of applications in the pharmaceutical industry, environmental monitoring, chemical war agent (CWA) detection, petroleum distillation, clinical chemistry, and food processing. In any of these cases, rapid and reliable response, low power consumption, and small size are critical system requirements.

In a GC system, Figure 1.1 , the mixture to be separated and analyzed is vaporized and injected into a separation column whose walls are coated by a polymer called stationary phase (Figure 1.2). The mixture components traverse the length of the column in a mobile phase (i.e. carrier gas) at rates determined by their retention in the stationary phase. If the column length and difference in the retention times are sufficient, a complete separation of components is possible. The separated components pass over a detector such as a flame ionization detector (FID), which generates a signal called chromatogram. The position of peak maximum on the chromatogram qualitatively identifies the component and the peak area is corresponding to the mass of the component present in the sample [4, 8].

1.2 On-Chip GC

Conventional GCs provide accurate analysis of complex mixtures but at the cost of using large, power-hungry, and relatively expensive table-top instruments (Figure 1.3). Furthermore, for some applications such as environmental monitoring and toxic/explosive compounds detection, this laboratory analysis is not proper due to demand of on-site fast response to the analytical results and the possibility of decomposition, loss and contamination of sample during its transportation. Therefore, a portable GC system is becoming increasingly important. MEMS technology has already demonstrated the possibility of realizing micro gas chromatography systems (μGC)

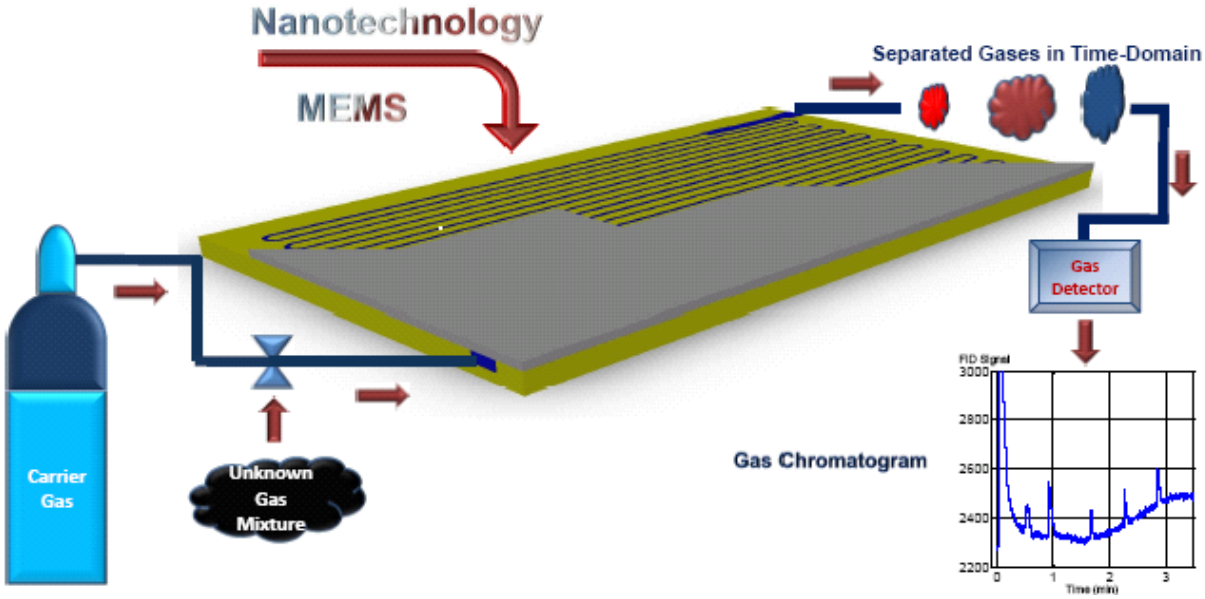

Figure 1.1 Schematic view of micro gas chromatography system.

which exhibit faster analysis times, lower power consumption, and higher portability compared to bulky conventional GCs [5, 6, 9-22]. A μGC system is a hybrid integration of several micromachined modules such as a preconcentrator (PC), separation column, gas detector, micro valves and pumps. The design and optimization of each individual module is the current trend in μGC development [7, 23-28].

The first μGC was reported on 1979 by Stephen Terry and co-workers at the Stanford Electronic Laboratory[3, 14]. This report illustrated the design, fabrication and characterization of a gas

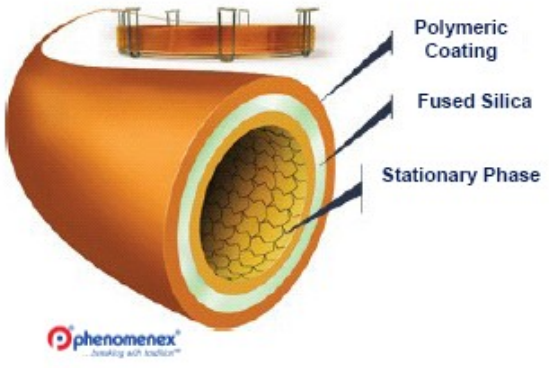

Figure 1.2 Schematic view of conventional separation column[1].

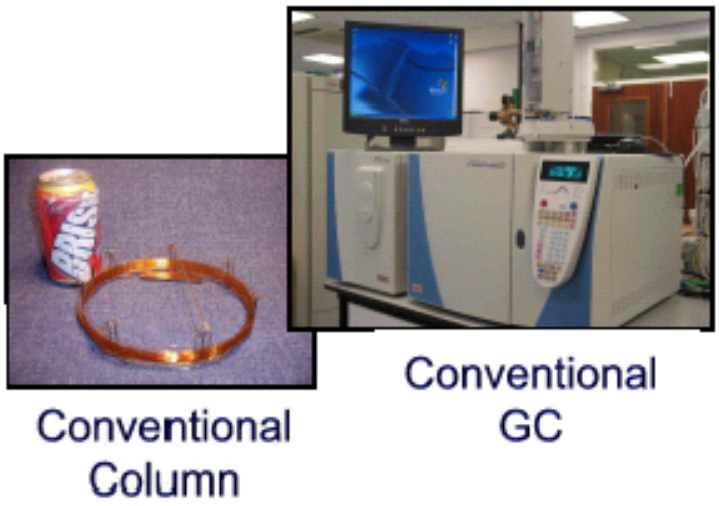

Figure 1.3 Conventional GC system and seaparation column[2].

chromatography system integrated on a silicon wafer. As shown in Figure 1.4, this device, which included a sample injection system, a 1.5m column and a thermal conductivity detector, was fabricated using standard photolithography and wet etching techniques. A Pyrex wafer was anodically bonded to the structured silicon wafer to create an enclosed separation column. Then the internal surface of the separation column was coated by standard OV-101 liquid stationary phase dissolved in a volatile solvent. Using the Helium as the carrier gas, the completed device was characterized by separating and detecting gaseous hydrocarbon mixtures in several seconds. Although it was a well-designed

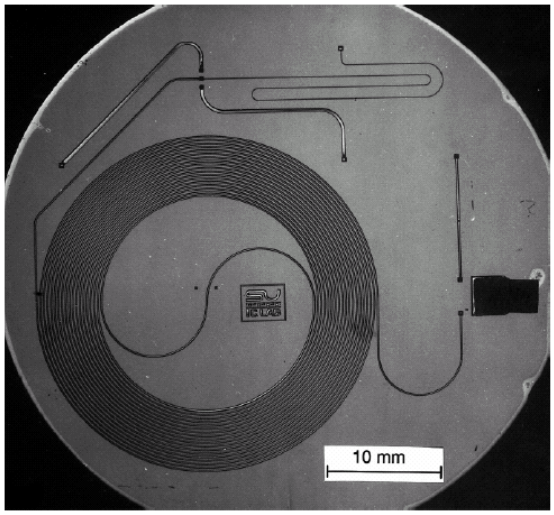

Figure 1.4 Photo of the integrated micro gas chromatography system by Terry and coworker at Stanford, 1979[3].

device, the system operation was not comparable to the conventional systems due to the poor separation performance of the column. The authors tried to improve the separation performance by decreasing the column depth at the expense of higher pressure drops. Unfortunately, the poor performance was originated from stationary phase deposition technique. In this technique, the pre-fabricated column was filled with the stationary phase solution, and then solvent evaporation caused the deposition of a layer of stationary phase. The condensation at the corners and curvatures resulted in a non-uniform and non-conformal coverage and thus poor column performance. Consequently, subsequent efforts to create μGC systems have mainly focused on the development of coating techniques capable of depositing a conformal layer of stationary phase inside the separation columns.

Edward Kolesar and Rocky Reston reported the first functional μGC systems on 1994[10, 15]. Their device incorporated a miniature sample injector, a 90cm long column with rectangular cross-section (depth: 10μm, width: 300μm), chemiresistor detector and a thermal conductivity detector (TCD). As the main contribution of this work, the stationary phase material was deposited onto the column walls prior to the bonding process. The 200nm-thick layer of

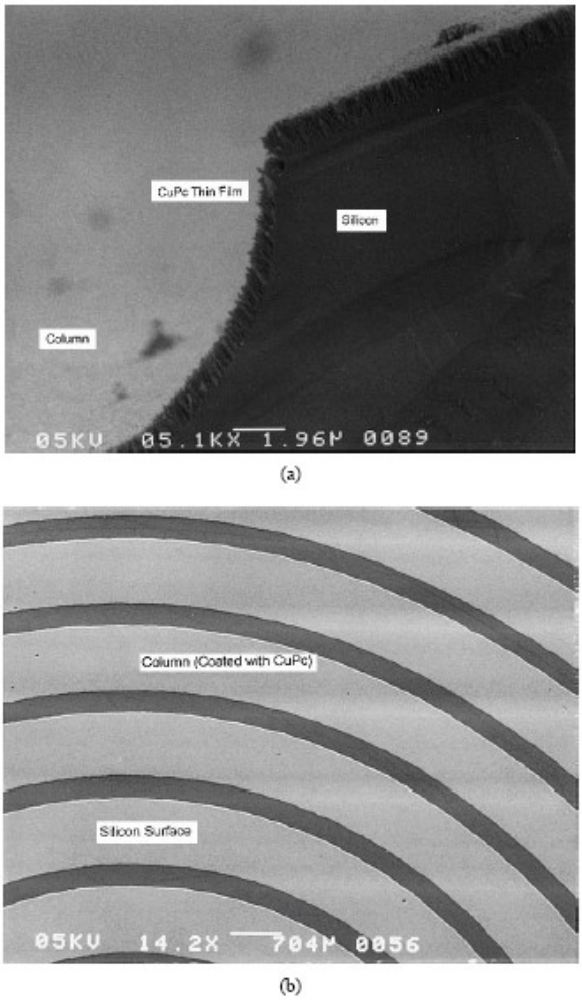

Figure 1.5 SEM image of the CuPc-coated μGC colum. (a) Column before the CuPc coating was removed from the flat surface regions (intra-column) (b) Column after the CuPc coating was removed from the flat surfaces required to accomplish the electrostatic bonding process with the Pyrex cover plate[6].

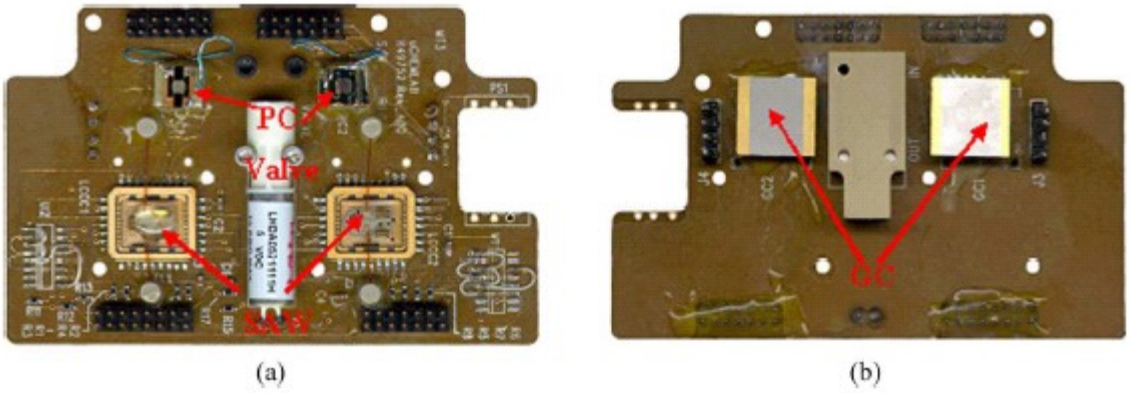

Figure 1.6 Hybrid integration µGC.. (a) Top and (b) bottom of the circuit board are shown. Two analysis channels are evident. The GC chip is 12 by 12 mm[7].

copper phthalocyanine layer was deposited all over the etched silicon wafer and then the top flat surface was polished using conventional IC patterning technique (Figure 1.5). Then this polished surface was anodically bonded to Pyrex wafer in order to create the enclosed separation column. This fabrication process ensured the creation of conformal stationary phase within the micro channels. However, the proposed stationary phase material was not able to afford the performance of the conventional polymer-based stationary phases and authors showed a poor separation of ammonia and nitrogen dioxide obtained using this device.

These promising achievements toward creating a portable instrument for on-site chemical measurements with national security applications such as the detection of biological and chemical war agents and pollution controls, motivated Sandia National Laboratories to initiate funding of a 'Microanalytical Systems" program in 1996. A significant part of this program had focused on the creation of µGC technology. The resulted device from this effort included a number of distinct micromachined components such as a microfabricated sample injector, pre-concentrator, a chromatographic polymer-coated column, and surface acoustic wave (SAW) detectors (Figure 1.6)[7]. The sample pre-concentrator included a sol–gel coated membrane and resistive heater to afford rapid sample heating. Since, the membrane had a small thermal mass it could be heated to 200 °C within 10 ms, resulting in concentration enhancements of over 2 orders of magnitude.

The chromatographic column was etched in silicon and coated with a thin-film of stationary phase material. Finally, the detection of separated species was performed using an array of chemically modified SAW sensors. This integrated system has been shown to successfully separate and detect a wide range of chemical species at parts per billion concentrations.

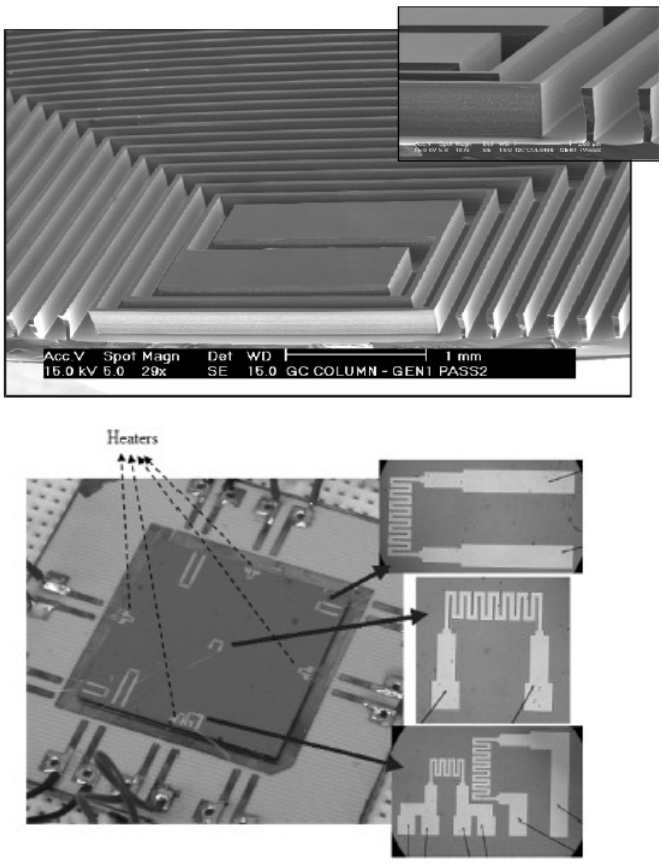

Figure 1.7 The 150µm wide, 250µm deep, 3-m long microchannels formed by DRIE in silicon (top). silicon substrate containing integrated heaters and temperature sensors(bottom)[5].

In 2005, Agah and coworker from University of Michigan reported a silicon-glass µGC column having integrated heaters and temperature sensors for flow control[5]. These 3m-long, 150µm-wide and 250µm-deep columns, integrated on a 3.3cm square die, were fabricated in silicon by anisotropic deep reactive ion etching (DRIE) and then were sealed by a Pyrex wafer (Figure 1.7). High-aspect-ratio rectangular cross-sectional channels with precisely controlled dimensions could be obtained by these processes. The integrated heaters afforded 40^{o}C/min temperature programming while consuming 650mW power. The authors continued their work by utilizing the buried-channel technique to fabricate rounded cross-section (25cm-long and 65µm-ID, Figure 1.8) columns on a 6mm-square chip[4]. The proposed fabrication method, which was CMOS compatible, significantly reduced the column mass and heater power consumption by more than one order of magnitude. However, the mechanical stability of the released column especially under the vacuum conditions

required to coat the column was a limitation of this method. Therefore, the separation performance of the coated column was not evaluated.

Finally, µGC columns as the heart of the system are still a technical challenge in order to realize a functional µGC system. This challenge is the major motivation of the work presented here. In Chapter 2, we introduce the concept of multi capillary columns and showed theoretically and experimentally that these columns, as well as ultra-narrow single capillary columns, can achieve fast separation of gas mixtures with high resolution suitable for on-site applications [29, 30]. In Chapter 3, we overcome the stationary phase coating problem by introducing a novel method named monolayer protected gold "MPG". The performance of this method is evaluated by coating different columns and separating polar and non-polar gas mixtures[16]. The last chapter introduces the future possible trends to develop the µGC system based on the fabrication technique presented in this work.

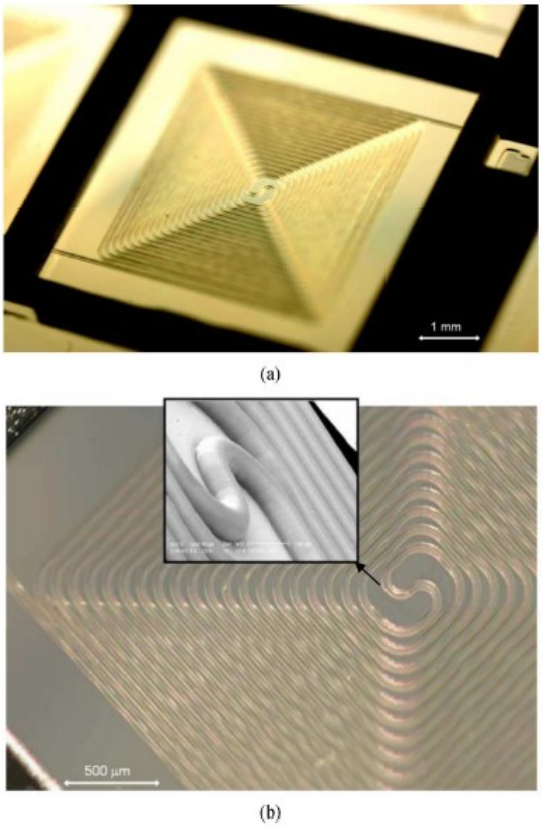

Figure 1.8 (a) Released 25-cm-long PECVD oxynitride column fabricated on a 6-mm-square die. (b) Optical image of the column with an SEM close-up image[4].

2 High-Speed μGC

2.1 Introduction

The development of high-speed and high-performance separation columns as the heart of the system is of paramount importance in the world of μGC for on-field applications such as environmental monitoring, breath analysis, and public safety. The reported MEMS-based columns for high-speed GC (HSGC) have achieved separation of a few analytes in seconds, but they have not been able to demonstrate highly efficient separations (complex mixture analysis) due to their significantly reduced column length (<50 cm) and their large channel width (>100 μm) [31-46]. This chapter addresses this situation by first demonstrating the successful design, fabrication, and stationary phase coating of very narrow-width columns (<30 μm), which yield the highest separation efficiency reported to date on MEMS-based GCs. A new class of microfabricated columns called multicapillary, consisting of a bundle of very narrow-width rectangular capillaries working in parallel, is also reported. The presented multicapillary columns enhance sample capacity and alleviate the stringent requirements on the amount of analyte that can be analyzed when using only a single narrow-width capillary column.

2.2 Theory

2.2.1 Single Capillary Column (SCC)

Analysis time, separation efficiency, and sample capacity are the main factors that need to be considered in the design and development of μGC columns for real-time trace analysis. Analysis time for a mixture is defined by the retention time, $t_{R,}$ of the last target component peak to elute from the column [47, 48]:

$$t_R = \frac{L}{u}(k+1) \tag{2.1}$$

where u is the average linear carrier gas velocity, L is the column length, and k is the retention factor for the component, which depends on column temperature and stationary phase properties. For a given column cross section, the retention time can be decreased by operating at (1) a higher carrier gas velocity, (2) a higher temperature, or (3) using a

shorter column. MEMS technology affords very high temperature programming rates (~600 ^{o}C/min) using on-chip heaters for ultra-low mass short separation columns [31, 33]. The major difficulty of using short columns for HSGC is the significant loss in column separation power. This amplifies the importance of using conditions that provide the maximum possible column efficiency.

The efficiency of GC columns is expressed by the height-equivalent-to-a-theoretical-plate (*HETP*). For rectangular channels, *HETP* is given by [49]:

$$HETP = \frac{2D_g}{u} f_1 f_2 + \left[\frac{\left(1 + 9k + 25.5k^2\right)}{105\left(k+1\right)^2} \frac{w^2}{D_g} \frac{f_1}{f_2} + \frac{2}{3} \frac{k}{\left(k+1\right)^2} \frac{\left(w+h\right)^2 d_f^2}{D_s h^2} \right] u \qquad (2.2)$$

where D_g and D_s are the binary diffusion coefficients in the mobile and stationary phases, respectively, d_f is the stationary phase thickness, w and h are the channel width and height, respectively, and f_1 (varies between 1 and 1.125) and f_2 (varies between 0 and 1) are the Gidding-Golay and Martin-James gas compression coefficients, respectively. Consequently, the number of theoretical plates (N) can be calculated using *HETP* value:

$$N = L / HETP \qquad (2.3)$$

Considering the second term in equation (2.2), it becomes clear that narrower columns (smaller w) provide a smaller HETP or better separation efficiency. For columns coated with a thin layer of stationary phase, the D_s term in equation (2.2) becomes negligible. Under this criterion, which applies to the columns presented in this report as well, the differentiation of the *HETP* equation leads to equations (2.4) and (2.5) showing the optimal average carrier gas velocity needed to achieve the maximum efficiency. From this equation, it is concluded that u_{opt} increases as the column becomes narrower:

$$HETP_{\min} = w\sqrt{8 f_1^2 \times \frac{\left(1 + 9k + 25.5k^2\right)}{105\left(k+1\right)^2}} \qquad (2.4)$$

$$u_{opt} = \frac{D_g f_2}{w} \sqrt{\frac{210\left(k+1\right)^2}{\left(1+9k+25.5k^2\right)}} \tag{2.5}$$

According to the above equations, reducing the column length to implement HSGC columns should be accompanied with a reduction in the channel width in order to achieve high-performance columns for complex mixture separation [31]. Moreover, as evident from equation (2.2), the slop of the *HETP* curve for $u > u_{opt}$ becomes proportional to w^2. This is important because in GC, the average linear carrier gas velocity is usually set above u_{opt} [50]. Therefore, a narrower column has a flatter *HETP* curve and provides higher flexibility during operation since its separation efficiency degrades less at higher velocities. As seen in equations (2.4) and (2.5), $HETP_{min}$ and u_{opt}, the optimum conditions for rectangular μGC columns, are independent of the channel depth. However, the channel depth can be increased to increase the column cross sectional area. This will enhance the sample capacity (see below) and volumetric flow rate without affecting the column performance and the separation time.

The downside of using HSGC columns with small widths is that for a given stationary phase thickness, the sample amount that can be injected without overloading the column is limited to several nano grams. This maximum sample amount, called sample capacity, is proportional to the effective volume of one theoretical plate, V_{eff}. This effective volume can be estimated by the following equation [51]:

$$V_{eff} = \left(1+k\right)\frac{V_G}{N} \tag{2.6}$$

where V_G is the gas-phase volume which can be calculated from the column dimensions. According to this equation, sample capacity drastically drops for narrow-width columns having a small cross-section area and small *HETP* (large *N*) [52]. Increasing the stationary phase thickness will increase the retention factor and sample capacity [51] with the expense of reducing separation efficiency according to equation (2). Furthermore, thick stationary phase coating will not improve the sample capacity for early eluting peaks with small retention factors (k<1) [51]. Another limitation of narrow-width

columns is that the volumetric flow rate can be very low [48], which in turn puts limitations on the detector sensitivity. The following section addresses these problems by introducing the first generation of MEMS-based multicapillary columns.

2.2.2 Multicapillary Column (MCC)

The idea of multicapillary columns was introduced by Golay in 1975 to increase the column separation efficiency without sacrificing sample capacity [47]. The main concept is that the reduced sample load, caused by using narrow-bore fused silica capillary columns, is compensated by increasing the number of capillaries, n, which work in parallel. Therefore, the sample capacity and flow rate can be theoretically increased by a factor of n. The *HETP* for a GC column is defined by the following equations [48]:

$$HETP = L\frac{\sigma^2}{t_R^2} \tag{2.7}$$

where σ^2 is the peak variance. As shown in Appendix A, *HETP* for MCCs can be defined in terms of the performance of its single capillaries, the stationary phase properties, and the structure features. In order to model the performance of MEMS-based MCCs, total peak variance (σ^2), and average retention time (t_R) should be calculated to find the value of *HETP* and plate number from equations (2.4), (2.5) and (2.7), respectively. Most of the detectors used for GC generate an electric signal, which is proportional to the amount of sample arrives at the detector through the carrier gas. This sample amount is related to the sample concentration in the carrier gas, C_s, and volumetric gas flow, $a \times u(a)$. Also, in the case of MCC, the total amount of sample arrives at the detector is a summation of the sample amount obtained from each single capillary in the bundle. According to these concepts, the average retention time is defined as[53]:

$$t_R = \frac{\int t(a)\, a\, u(a)\, P(a)\, da}{\int a\, u(a)\, P(a)\, da} \tag{2.8}$$

where $t(a)$ and $u(a)$ are the retention time and the average carrier gas in a single capillary with cross-section area of a. $P(r)$ is the Gaussian function of the area distribution.

$$P(a) = \frac{1}{\sqrt{2\pi}\sigma_a}\left[-\frac{(a-a_o)^2}{2\sigma_a^2}\right] \tag{2.9}$$

Substituting Eq. (2.9) into Eq. (2.8), expanding *t(a)* into the Taylor series near a_o, and considering the first term of the expansion, it can be obtained that:

$$t_R = t(a_o) = \frac{L}{u_o}(k_o + 1) \tag{2.10}$$

The minimum value for the MCC peak variance is equal to the peak variance of the single capillary. However, the inhomogeneity of capillaries causes different volumetric flow and consequently increases the peak variance. According to this concept, we have:

$$\sigma^2 = \sigma_o^2 + \langle(\Delta t)^2\rangle \tag{2.11}$$

where σ_o^2 is the peak variance of a single capillary, which can be calculated by the Golay equation [48]. The second term, which is the average of the peak time differences, models the band broadening caused by the distribution of retention times resulting from each capillary in the bundle [23]:

$$\langle(\Delta t)^2\rangle = \frac{\int (t(a)-t_R)^2\, a\, u(a)\, P(a)\, da}{\int a\, u(a)\, P(a)\, da} \tag{2.12}$$

To evaluate Eq. (2.12), t_R should be replaced with Eq. (2.10) and *k(a)* and *u(a)* should be extended in terms of dimensions of the capillaries and coating method properties. For laminar flow resulting from a constant pressure drop, we have

$$u(a) = u_o a / a_o \tag{2.13}$$

The retention factor is proportional to the ratio of the volumes of the stationary and gas phases and for a rectangular capillary:

$$k(a) = V_l / V_g = 2K \frac{w+h}{wh} d_f \tag{2.14}$$

where K is the distribution coefficient and d_f is the stationary phase thickness, which can be estimated as a function of coating solution concentration and capillary dimensions:

$$d_f = \frac{C_{cs}}{\rho_{stationary}} \left(\frac{wh}{2(w+h)} \right)^{\alpha} \tag{2.15}$$

Often the method and environmental conditions of coating process determine the experimental value of α. Substituting Eq. (2.10), (2.13), (2.14), (2.15) into Eq. (2.12) and using Taylor series yield:

$$\langle (\Delta t)^2 \rangle = \frac{L^2}{u_o^2} \left[\frac{1 + k_o \dfrac{2 - \alpha + h_o / w_o}{1 + h_o / w_o}}{1 + k_o} \right]^2 (\frac{\sigma_h}{h_o})^2 + \frac{L^2}{u_o^2} \left[\frac{1 + k_o \dfrac{2 - \alpha + w_o / h_o}{1 + w_o / h_o}}{1 + k_o} \right]^2 (\frac{\sigma_w}{w_o})^2 \tag{2.16}$$

Finally, the following expression for the *HETP* of a rectangular cross-section multicapillary column can be achieved by using (2.4), (2.5), (2.10), (2.11)and (2.15):

$$\begin{aligned} HETP = \frac{u_o^2}{L[1+k_o]^2} \sigma_o^2 + L \left[\frac{1 + k_o \dfrac{2 - \alpha + h_o / w_o}{1 + h_o / w_o}}{1 + k_o} \right]^2 (\frac{\sigma_h}{h_o})^2 \cdots \\ + L \left[\frac{1 + k_o \dfrac{2 - \alpha + w_o / h_o}{1 + w_o / h_o}}{1 + k_o} \right]^2 (\frac{\sigma_w}{w_o})^2 \end{aligned} \tag{2.17}$$

In static coating method, used in this paper, coating thickness can be calculated by dividing the polymer volume dissolved in the solvent by the total inner surface of capillaries (see below). Assuming this value for coating thickness and using Eq. (2.14), coating constant (α) have the value of one. It simplifies the *HETP* equation in (2.17):

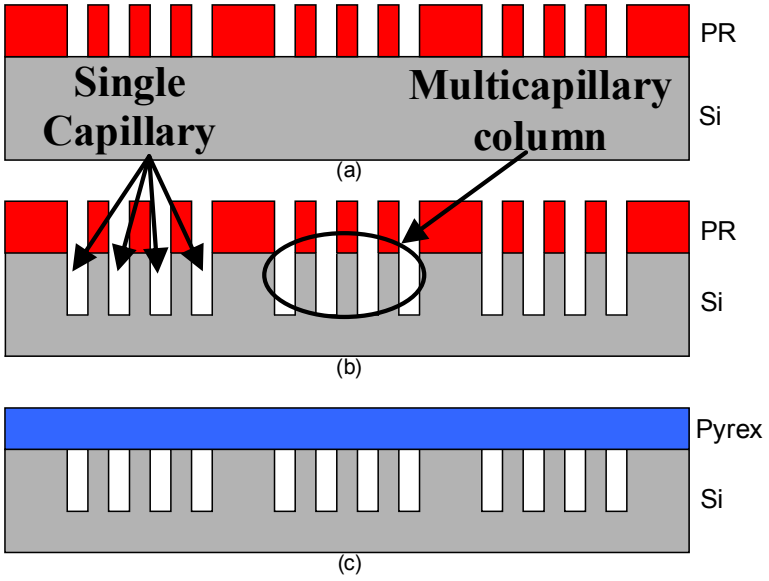

Figure 2.1 Fabrication process flow for MEMS-based multicapillary columns. The column formed from silicon wafer etched using deep reactive ion etching (DRIE) technique (a-b) and bonded to a Pyrex wafer(c)

$$HETP = \frac{u_o^2}{L[1+k_o]^2}\sigma_o^2 + L(\frac{\sigma_h}{h_o})^2 + L(\frac{\sigma_w}{w_o})^2 \qquad (2.18)$$

In this equation, the first term, which is called $HETP_o$, refers to the *HETP* of a capillary whose dimensions are the average of the dimensions of all capillaries in the bundle and can be calculated from equation (2.2). The second term is related to the band broadening caused by inhomogeneity of the channels. If all the capillaries in the bundle have exactly the same dimensions ($\sigma_h = \sigma_w = 0$), the second and third terms of the MCC performance equation would be zero, which means that MCC has an *HETP* equal to that of the single capillary while its sample capacity is multiplied by the number of capillaries in the bundle. Conventional MCCs comprising a bundle of round capillaries show a dispersion of 3-4% [53]. As shown later, highly homogenous rectangular capillaries can be fabricated by MEMS technology in order to minimize the second and third term in equation (2.18) and to increase the separation performance.

2.3 Design, Fabrication and Stationary Coating

2.3.1 Column Design and Fabrication

In order to study the width effect on *HETP*, SCC columns with four different capillary widths (25, 50, 125, and 250 μm) were designed. Moreover, two-, four- and eight- capillary MCCs were fabricated to characterize the MCC performance. All the columns had a length of 25 cm and all the MCCs had a constant total width of 250 μm. The fabrication of both silicon-glass SCCs and MCCs started with cleaning a silicon wafer in a Piranha solution. Then, a 10 μm-thick layer of AZ9260 photoresist was spun on the wafer at 3k rpm for 60 seconds. After patterning the photoresist (Figure 2.1.a), the wafer was etched to a depth of 250 μm using deep reactive ion etching (DRIE) technique to form channels with aspect ratios varying between 1 (for 250 μm-wide columns) and 10 (for 25 μm-wide columns) (Figure 2.1.b). After stripping the resist, the silicon wafer was anodically bonded to a Pyrex 7740 substrate (Figure 2.1.c) at the temperature and pressure of 350 ^{o}C and 2k Pa, respectively, using a DC voltage of 1250 V. The wafers were kept under these conditions until the leakage current was less than 1 mA. The final step is dicing the wafer to form 10 × 8 mm^2 chips, a picture of which is shown in Figure 2.3. In order to connect the chips to the GC system, fused silica capillary tubing with 167-μm-O.D. and 100-μm-I.D. was used.

Figure 2.2 shows SEM images of SCCs and MCCs before the channels were sealed and also a broken sealed column. As can be seen, we have used the serpentine architecture for the design of both SCCs and MCCs. As recent studies confirm [54], the serpentine configuration is preferred over the spiral one in the design of μGC columns as it minimizes the number of corners per channel length and its even number of corners in clockwise and counterclockwise directions compensates the peak broadening caused by turn effect. Moreover, the serpentine design equalizes the length of all the capillaries in the MEMS-based MCC[55]. This is a crucial characteristic for ensuring high-efficient separation which cannot be achieved by the spiral design.

It is also important to divide the carrier gas equally between the capillaries in MCCs such that the same analytes in all capillaries travel the column length with the same velocity before merging again at the column outlet. For this reason, as shown in Figure

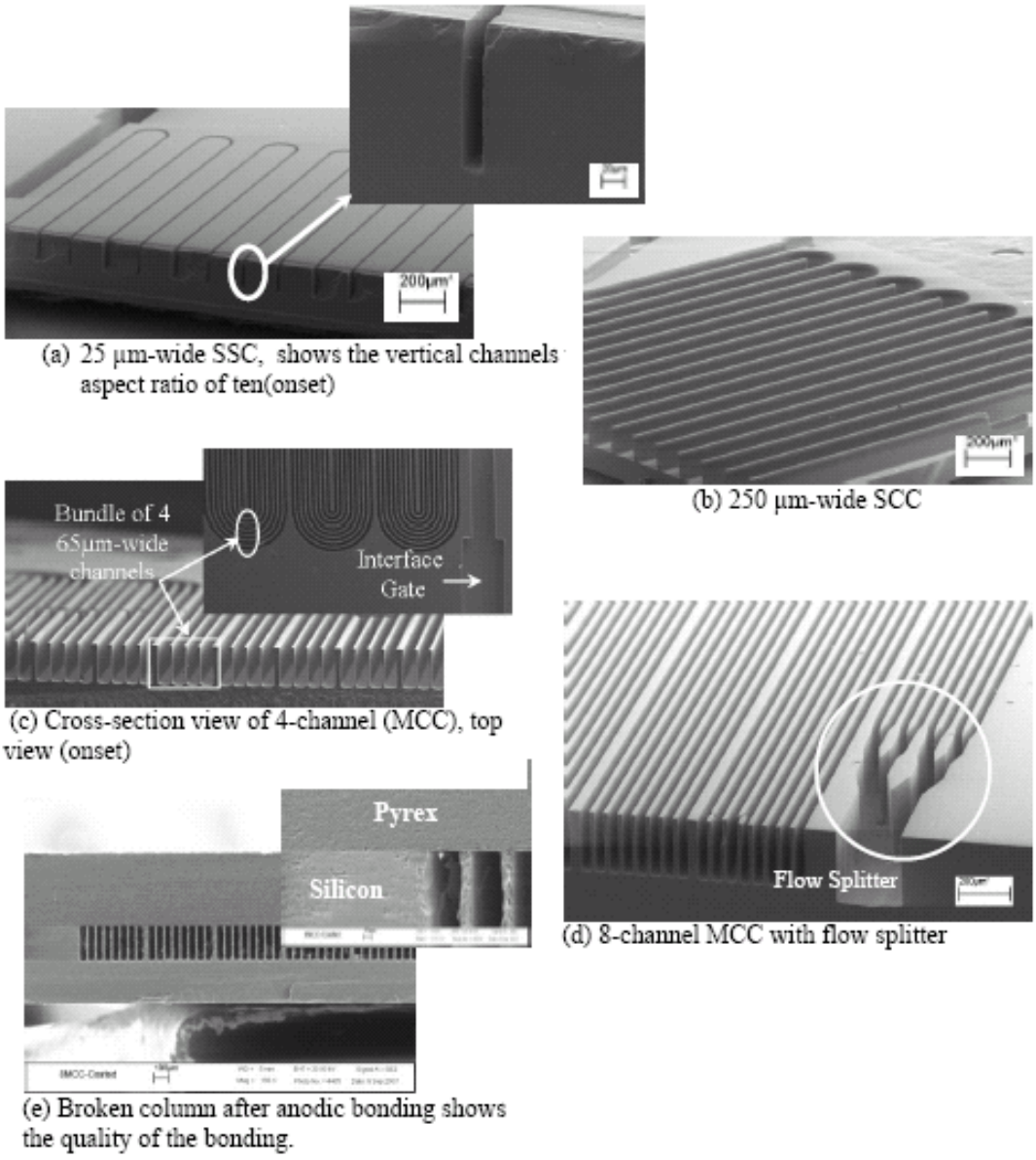

Figure 2.2 SEM images, (a-d): broken columns before anodic bonding, (e) broken column after anodic boning shows the bonding quality.

2.2, flow splitters have been implemented at the inlet and outlet of MCCs. The effectiveness of the flow splitter was studied by simulating the injection of a 1 mm-wide sample plug of methane at a carrier gas velocity of 20 cm/s and then measuring the plug width after passing through the 1 cm-long channel with and without a splitter. This

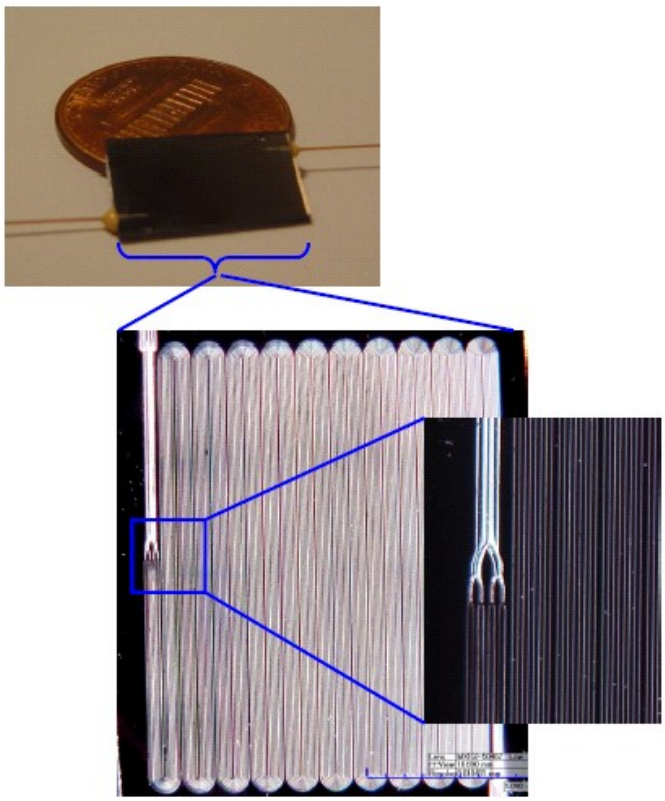

*Figure 2.3 Optical images. 8-channel MCC column fabricated on an 8*10 mm square die after anodic bonding shows the serpentine design of the column and flow splitter.*

simulation showed the plug width is almost 20% less in the case of flow splitter. As Figure 2.4 demonstrates, this improvement is related to the equal distribution of the sample molecules between the capillaries as a result of the multi-step flow splitter configuration. It is worth to mention that the Reynolds number is less than in all the experiments, consequently the flow is laminar.

2.3.2 Stationary Coating

The major challenge in stationary phase coating of the MEMS columns is to obtain a uniform film throughout the column length. The static method has been applied in this work to achieve the highest possible separation efficiency and resolution. For these rectangular MEMS columns, similar to round fused silica capillary columns, the

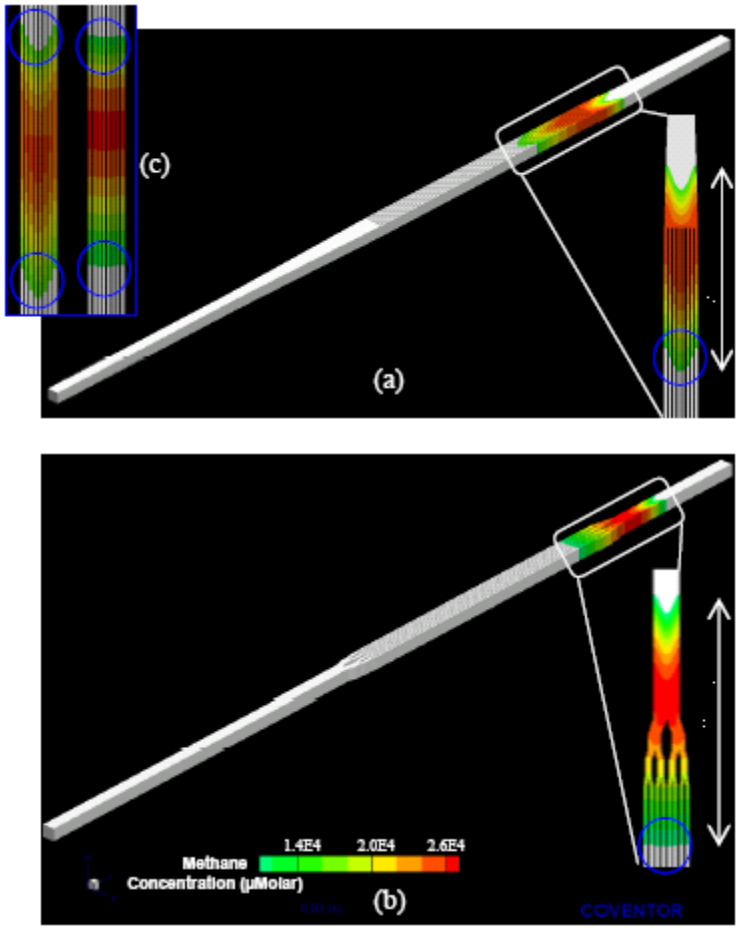

Figure 2.4 Contour plot of injected sample concentration (µMolar), (a) and (b): plug is passing the input gate; (c) plug is traveling in the capillaries. The output plug in the column with flow-splitter (b and c right) is 20% narrower than that without flow-splitt (a and c left) due to the uniform distribution of the sample molecules. The parabolic profile of the sample concentration contour becomes flat by using flow splitter (blue circles).

thickness of the stationary phase achieved by static coating can be easily calculated by dividing the total coating mass dissolved in the solution by the total column internal surface. This thickness, d_f, can be calculated by:

$$d_f = \frac{C_{cs}}{2\rho_{statinary}} \frac{1}{(\frac{1}{w} + \frac{1}{h})} \tag{2.19}$$

where C_{cs} and $\rho_{stationary}$ are the coating solution concentration and stationary phase density, respectively. The following details of coating method have been used to deposit a uniform stationary phase with identical thickness for all the columns. However, a range of 0.1-0.4 μm thickness has been estimated due to the variation of environmental conditions and experimental inaccuracy.

The tubing was first deactivated at 400 °C with octamethylcyclotetrasiloxane (D4) as the deactivation agent using a previously published procedure [56]. After deactivation, the tubing was washed with 0.5 mL of methylene chloride and then purged with helium at 220 °C for 60 minutes. The tubing was then attached to the microfluidic ports of the chip using two-part adhesive (Epoxy 907, Miller-Stephenson). The deactivation procedure was repeated a second time to ensure deactivation of the chip. Due to temperature limitations of the epoxy, the deactivation procedure was performed at 250 °C, instead of 400 °C, for 90 minutes. The washing and purging procedures were also repeated. Then, a solution of polydimethylsiloxane (OV-1) dissolved in n-pentane was used to fill the column while one end of the column was blocked by pushing a small amount of wax into the capillary tubing. The concentration of the coating solution was calculated in the range of 4 mg/ml and 8 mg/ml for different designs in order to achieve an optimum coating thickness. A vacuum was then applied to the other end while the column was kept in a water bath at 35 °C. This resulted in slow evaporation of the solvent leaving behind a thin layer of stationary phase on the column walls. In order to obtain a stable film, the OV-1 stationary phase was cross-linked by passing a vapor of azo-tetrabutane (AZT) through the column for 60 minutes. Finally, the column was sealed at both ends and heated at 220 °C for 60 minutes. It should be noted that no leakage was observed during column coating indicating the anodic bond integrity. The effect of the surface imperfection on the bonding quality was determined by Anthony[57]. However, anodic bonding is the most commonly used method for joining silicon to Pyrex[58]. The bonding conditions were optimized to prevent any effective leakage which might affect the column performance.

2.4 Results and Discussion

In order to evaluate the capabilities of the microfabricated columns, several experiments were conducted using conventional GC system (5890 Series II GC, Hewlett Packard) having a split inlet (200:1) and flame ionization detector (FID). The capillary column inside the GC was replaced by the MEMS column. The autosampler (7673B, Hewlett Packard) was used to inject the samples. Air was used as a carrier gas. All gases were purified with filters for water vapor and hydrocarbons. The injector and FID temperature were both maintained at 280 ^{o}C. In these experiments, methane was used to measure the average linear carrier gas velocity for its negligible interaction with the column and being known as an unretained compound on OV-1 stationary phase. Nonane was used to determine *HETP* because of having a retention factor more than 10, thus making *HETP* less dependent on the compound selected (k) and experimental conditions (mainly temperature). We used dodecane (k>10) to study the effect of analyte concentration on *HETP* and to measure sample capacity of different microfabrication columns. Due to having a higher diffusion coefficient (~16%) in the mobile phase (D_g) [50], u_{opt} of nonane is slightly more than that of dodecane according to equation (4). As mentioned earlier, the carrier gas velocity should be set slightly above u_{opt} during GC operation. Therefore, using dodecane at the optimum carrier gas velocity (u_{opt}) of nonane (determined from *HETP* characterization) satisfies this requirement.

2.4.1 Single Capillary Column (SCC)

Two important features of these microfabricated columns were investigated. First, to determine the separation efficiency, the *HETP* was measured by injecting a 1 µl mixture of nonane (C_9H_{20}) and methane (CH_4). The hold-up time of methane, t_M, was used to measure the average linear carrier gas velocity, u_{ave_column}, and the nonane peak was used to determine the *HETP* experimentally based on:

$$u_{ave\_column} = \frac{L + L_{TL}\left(A_t / wh\right)}{t_M} \tag{2.20}$$

$$HETP = \frac{L}{5.54\left(\frac{t_R}{w_h}\right)^2} \tag{2.21}$$

where A_t and L_{TL} are the cross sectional area and the length of the transfer lines (fused silica tube used to connect the μGC column to the FID) and w_h is the width of the peak at the half height. Only symmetric peaks (symmetry of 0.9-1.1) were used to measure *HETP*. All experiments were performed at least three times. The retention factor, $k\ (= t_R/t_M - 1)$, measured for nonane peaks had a value more than 10 in all the MEMS columns. According to equation (4), $HETP_{min}$ and u_{opt} are strongly dependent on retention factor for k<10 but they vary within 10% and 5%, respectively, when k>10. Therefore, the variation in the retention factor had negligible influence on *HETP,* making it an acceptable figure of merit for comparing the performance of different columns [48]. Figure 2.5 shows *HETP* as a function of the average linear carrier gas flow velocity for four different channel widths decreasing from 250 μm to 25 μm. The narrowest channel showed a 7. 9-fold improvement in the separation efficiency and 3.5-fold increase in the optimum flow velocity compared to the corresponding values for the widest column. The 25 μm-wide column yielded a minimum *HETP* of 0.008 cm (12,500 plates/m) at a linear gas velocity of 36 cm/s making it the highest efficient MEMS-based column reported to date [37]. As we expected according to the theoretical discussion in section 2.2.1, the *HETP* curve is flatter for the 25 μm-wide SCC. The 25 μm-wide SCC presented herein affords an *HETP* less than 0.02 cm over a wide range of flow velocities from 35 cm/s to 80 cm/s making it a suitable candidate for HSGCs. We need to add that the differences in the cross sectional areas between the μGC column and the transfer lines forces the carrier gas to be compressed at the μGC column inlet and expanded at the outlet. While this sudden expansion and compression causes negligible pressure drops for the laminar flow inside these micro-scale channels [59] they can increase band broadening and reduce the separation efficiency. We envision that 25 μm-wide columns can produce higher separation efficiencies when transfer lines are removed through the integration of the injector and detector with the μGC column. [60]. In spite of this issue and all the experimental errors, the improvement trend in *HETP* agrees with the mathematical

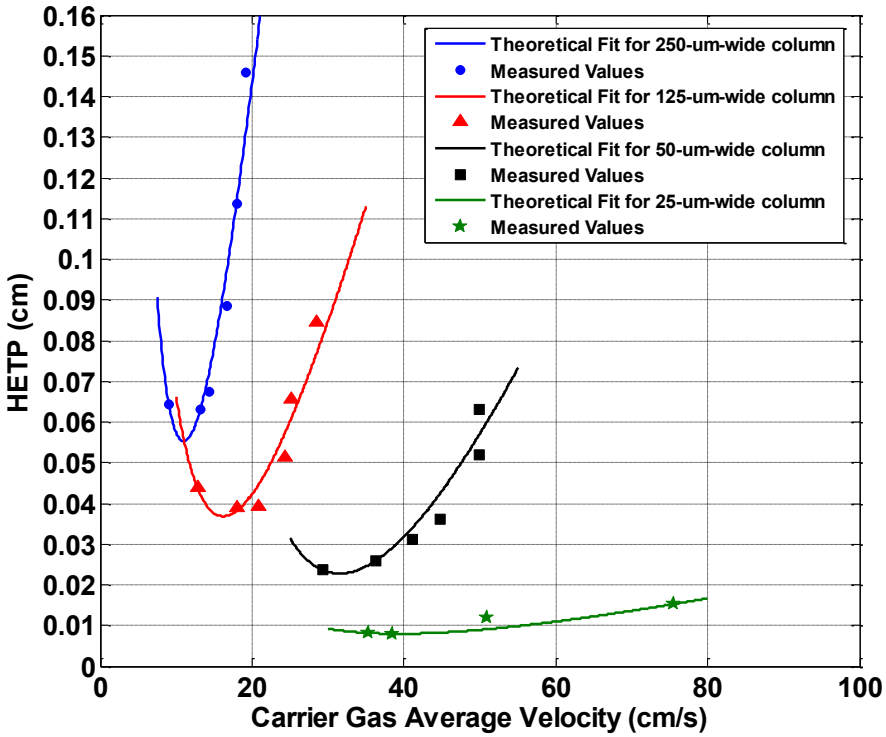

Figure 2.5 Golay plot for SCCs, measured using isothermal (30 °C) injection of nonane and helium as a carrier gas, showing the improvement trend in the separation efficiency and optimum carrier gas velocity by decreasing the channel width.

model. For instance, according to equation (2.4), we expected the 125 µm-, 50 µm-, and 25 µm-wide columns to have 2, 5, and 10 times smaller $HETP_{min}$ compared to the 250 µm-wide column. The empirical results show a factor of 3, 4.9, and 7.9, respectively (Figure 2.5).

To determine the sample capacity, solutions of dodecane ($C_{12}H_{26}$) in methylene chloride were prepared in increasing concentrations from 250 ng/µL to 10 µg/µL and the *HETP* was calculated for each sample by an injection of 1 µl of the solution at 60 °C with a split ratio of 200:1. The maximum sample amount without significant change in the *HETP* (less than 10%) was used to determine the column sample capacity. Table 2-1 lists the measured sample capacities of the columns. The wider channels provided a larger

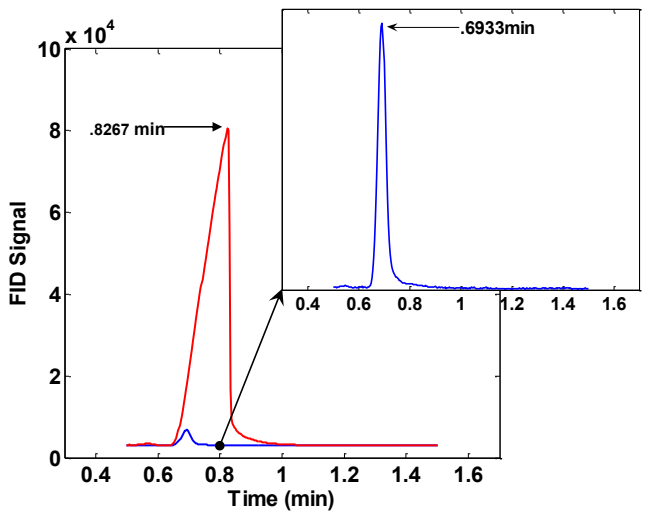

(a)

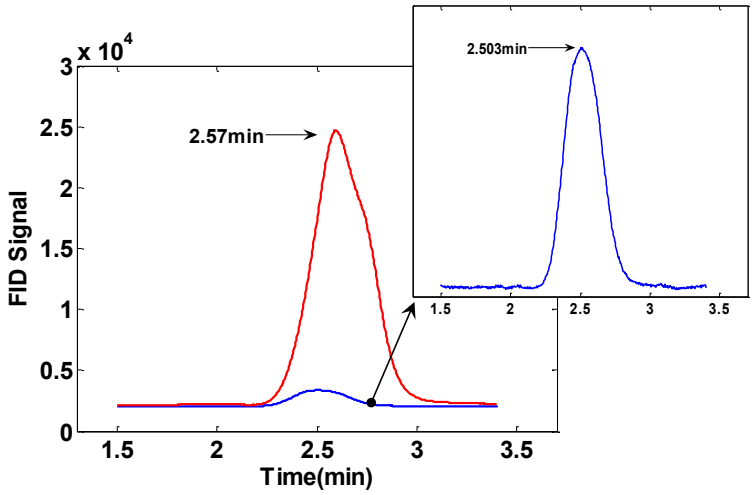

(b)

Figure 2.6 (a) 250µm-wide SCC, leading peak effect, caused 19.2% difference in the retention time for 10ng (blue) and 100ng (red) injection of dodecane at 60°C and helium as the carrier gas at 10psi column inlet pressure. (b) Four-capillary MCC, the retention time difference was 2.6% under experimental conditions.

surface in contact with mobile phase, increased the total stationary phase, and consequently the maximum sample capacity before overloading the column. The 25 µm-wide column has high performance but it is limited to very low amount of samples (5.5

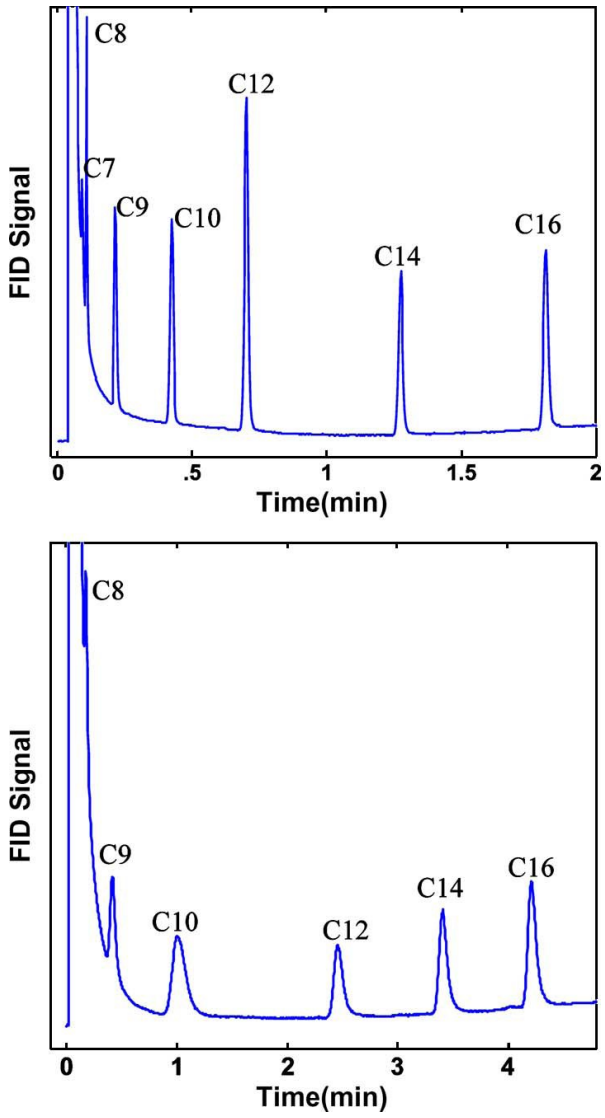

Figure 2.7 Chromatogram of a hydrocarbon mixture, obtained using a 25-µm-wide channel SCC (top) and four-channel MCC (bottom), 35 ^{o}C isothermal for the first one minute and then a temperature rate of 30 oC/min, helium as the carrier gas (Heptane eluted with the so solvent in MCC).

ng for dodecane). As evident in Figure 2.6a, if too much sample is introduced onto the column, "leading peak" will appear. These leading peaks are distorted, giving a slow rise to the peak and a fast drop. In this case, retention time increases and consequently the sample peak time increases. It means that quantitative analysis, which is based on the

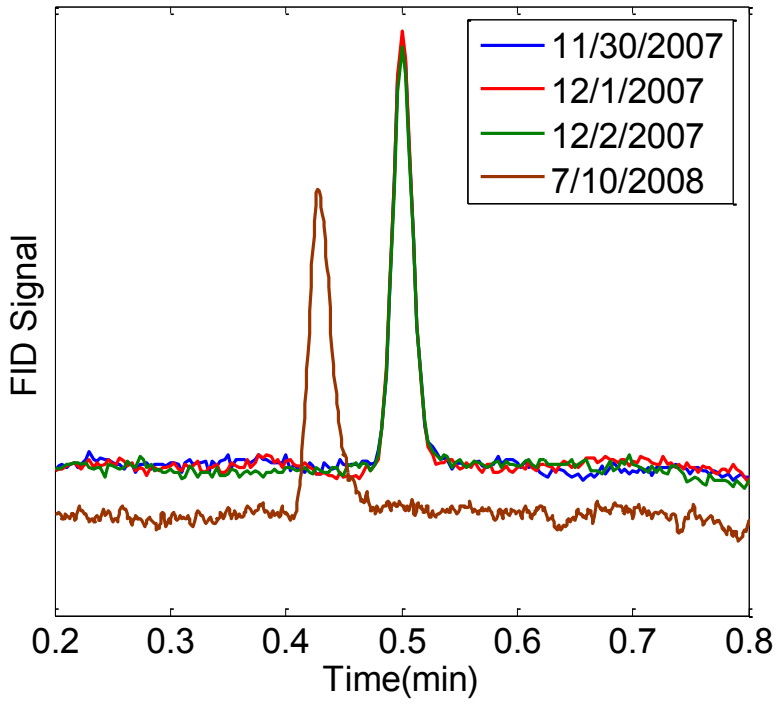

Figure 2.8 Long-term coating performance evaluation, chromatogram of nonane obtained using a 25-um-wide channel SCC. 35°C isothermal helium as the

comparison between peak time of the sample in a known mixture and unknown mixture, cannot be performed. This low sample capacity is a limitation of these high-efficient columns especially for in-field applications and the analysis of samples with unknown concentrations.

2.4.2 Multicapillary Column (MCC)

MCC columns are promising in that they can provide high efficiency of narrow columns while providing larger sample capacities. However, we need to acknowledge the fact that their stationary phase coating is more challenging especially for large number of narrow capillaries since all the capillaries in the bundle need to have the same coating thickness. We proposed a novel coating technology to overcome this challenge which is described in the future chapter. While the MEMS SCCs and 2-channel and 4-channel MCCs were successfully coated with OV-1 stationary phase using the static technique described earlier, this conventional method failed to produce robust coating on 8-channel

Table 2-1 Sample capacity, measured using dodecane injection at 60 ^{o}C, helium as the carrier gas.

Column Design-Channel width (μm)	***Sample Capacity (ng)***
SCC-25	**6**
SCC-50	**10**
SCC-125	**12**
SCC-250	**19**
MCC-125 (2-capillary)	**50**
MCC-65 (4-capillary)	**200**

MCCs consisting 30 μm-wide capillaries. Table 2-1 lists the sample capacity for columns successfully coated with OV-1. The columns having more capillaries demonstrate higher sample capacity. The MCC with four 65 μm-wide capillaries presented a much larger sample capacity (20 fold) compared to the 50 μm-wide SCC. Considering the same coating thickness and using experimental *HETP* for these two columns, the sample capacity improvement should be around 26 fold (see equation (2.6)). This small deviation between experimental results and theoretical expectations was mainly due to differences in the coating thickness and inaccuracy of the experimental measurements. As shown in Fig. 6b, an increase of the sample amount from 10 ng to 100 ng resulted in a 2.6% increase in the retention time of dodecane for the MCC. The change of dodecane retention time for the 50 μm-wide SCC under the same conditions was about 19%.

The separation performance of the SCCs and MCCs have been explored by separating a gas mixture containing n-alkanes (C7-C8-C9-C10-C12-C14-C16) (Sigma-Aldrich Inc., MO, US), in the conventional GC oven. Figure 2.7 shows the chromatogram obtained using a 25 μm-wide SCC and four-channel MCC at a 30 ^{o}C/min temperature programming rate. The high-performance SCC chromatogram obtained by an injection

Table 2-2 Statistical data, obtained by SEM images to characterize the homogeneity of channels in different microfabricated MCCs at different cross sections.

MCC	Statistical Data to qualify fabrication process						H_o cm	$L\left[\left(\frac{\sigma_h}{h_o}\right)^2+\left(\frac{\sigma_w}{w_o}\right)^2\right]$ mm
	Average channel width(W) μm	Average width dispersion $(\frac{\sigma_W}{W})\%$	Average channel depth(D) μm	Average depth dispersion $(\frac{\sigma_D}{D})\%$	Average cross-section area(A) $(\mu m)^2$	Average area dispersion $(\frac{\sigma_A}{A})\%$		
2-capillary	**126.5**	**0.27**	**256.7**	**0.43**	**32466**	**0.53**	**0.014**	**0.006**
4-capillary	**65.3**	**0.47**	**244.7**	**0.26**	**15983**	**0.51**	**0.009**	**0.007**
8-capillary	**36.2**	**0.52**	**231.4**	**0.19**	**8388**	**0.55**	**0.007**	**0.008**

volume of 0.5 µl and a split ratio of 1:200 shows 7 sharp peaks separated in less than 2 minutes. In MCC chromatogram, the injection volume was 2 µl with a split ratio of 1:20 which can easily overload all the fabricated SCCs. The separation time of 6 components was less than 5 min but it can be significantly reduced by using higher temperature programming rates via integrating on-chip heaters [32, 37, 45]. According to this comparison, 8-channel MCCs consisting of 30 µm-wide capillaries are capable of providing high performance separation similar to that of 25 µm-wide SCCs but at much higher sample concentration.

The coating stability was evaluated by monitoring the retention time and band broadening of the nonane peak over a time period of 8 months. As Figure 2.8 shows, the variation of t_R and w_h were less than 15% and 12%, respectively. These small variations considering the measurement errors show the high stability and reproducibility of the coating procedure.

Table 2-2 summarizes the channel dimensions and statistical dispersion factors for different microfabricated MCCs. The cross-sectional dispersion of these MEMS MCCs is about 0.5% and is significantly lower than that of conventional MCCs (3-4%) consisting of 500-1200 glass capillaries [53]. Considering equation ((2.18)) and according to Table 2-2, the peak broadening resulting from inhomogeneities in the capillaries' dimensions (second term of equation (2.18)) is one order of magnitude less than that from the peak broadening resulting from a single capillary (first term). These important results indicate

that the MEMS MCCs are highly homogenous and, hence, can achieve lower *HETP*s compared to their conventional counterparts in which the second term is the dominant contributor to band broadening, and hence, cannot yield efficiencies comparable to that of a single-capillary column.

The primary experimental measurements of minimum *HETP*, under the same conditions mentioned above, showed a value of 0.05 cm and 0.12 cm for two- and four-capillary MCCs, respectively. This deviation comparing to theoretical expectation (see Table 2-2) is mainly attributed to the nonunformity of the stationary phase coating. The novel coating technique, recently reported in [61, 62] based on self-assembly of nano-structured materials is promising to achieve a uniform thin layer of stationary phase in all the rectangular capillaries in the presented microfabricated MCCs.

2.5 Conclusion

This paper has presented the development of DRIE-Si/glass high-efficient μGC columns. The tradeoff between separation efficiency and sample capacity has been addressed by presenting the MCCs. The separation efficiency and sample capacity have been studied both theoretically and experimentally. General correlations for the efficiency of rectangular cross-section MCCs have been developed. The narrow SCCs provide high performance while MCCs present high sample capacity at the same time. The separation ability of SCCs and MCCs has been evaluated by an alkane mixture (C7-C8-C9-C10-C12-C14-C16) and the coating stability has been evaluated over a period of 8 months. The efficiency of such MCCs depends on the dispersion of the capillary dimensions in the bundle as well as the coating technique. The compatibility with unpredictable amount of environmental samples states MCCs' potential applications in environmental monitoring and homeland security. Developing novel coating methods to optimize the correlation between MCC efficiency and coating constant (α) can be the next step to achieve even higher efficiency.

3 Novel Stationary Phase Technology for μGCs

3.1 Introduction

μGC columns as the heart of the system are generally fabricated in silicon by anisotropic deep reactive ion etching (DRIE) and then are sealed by a Pyrex wafer. High-aspect-ratio rectangular cross-sectional channels with precisely controlled dimensions can be obtained by these processes. The columns are then coated by a thin layer of a polymeric stationary phase such as methyl silicones or poly(ethylene glycol) using conventional static or dynamic techniques. Recently, we introduced the concept of multi capillary columns and showed theoretically that these columns as well as ultra-narrow single capillary columns can achieve fast separation of gas mixtures with high resolution suitable for on-site applications [29, 30].

However, since the early μGC work, stationary phase coating of MEMS columns has been a challenging step in order to obtain reproducible and high resolution separations[63]. It is mainly because the conventional techniques relying on solvent evaporation can be utilized after separation channels are sealed [25-27]. These methods, which are developed for fused silica capillary tubing, cannot afford conformal coating in the rectangular-shaped μGC columns. They suffer from pooling effects and can easily plug the column during solvent evaporation especially as the column width is reduced to enhance the separation efficiency [29], examples of which are shown in Figure 3.1. Additionally, even for wide μGC columns, the thickness and surface properties of MEMS columns coated with conventional techniques are not easily adjustable. Thermal decomposition of these polymers due to heating and cooling cycles in temperature programmed μGC causes separation performance deterioration over time [8]. Furthermore, in order to achieve complete portability; μGCs have to operate with ambient air as carrier gas. Therefore, chemical composition of stationary phases should be stable in contact with air and humidity. Most common stationary phases such as polydimethiylsiloxane (PDMS) rapidly decompose in air and moisture, therefore are not suitable for μGCs [64, 65].

Recently, there has been a focus on developing new stationary phases for high speed gas separation applications [61, 62, 66-72]. Bare gold nanoparticles was used to improve

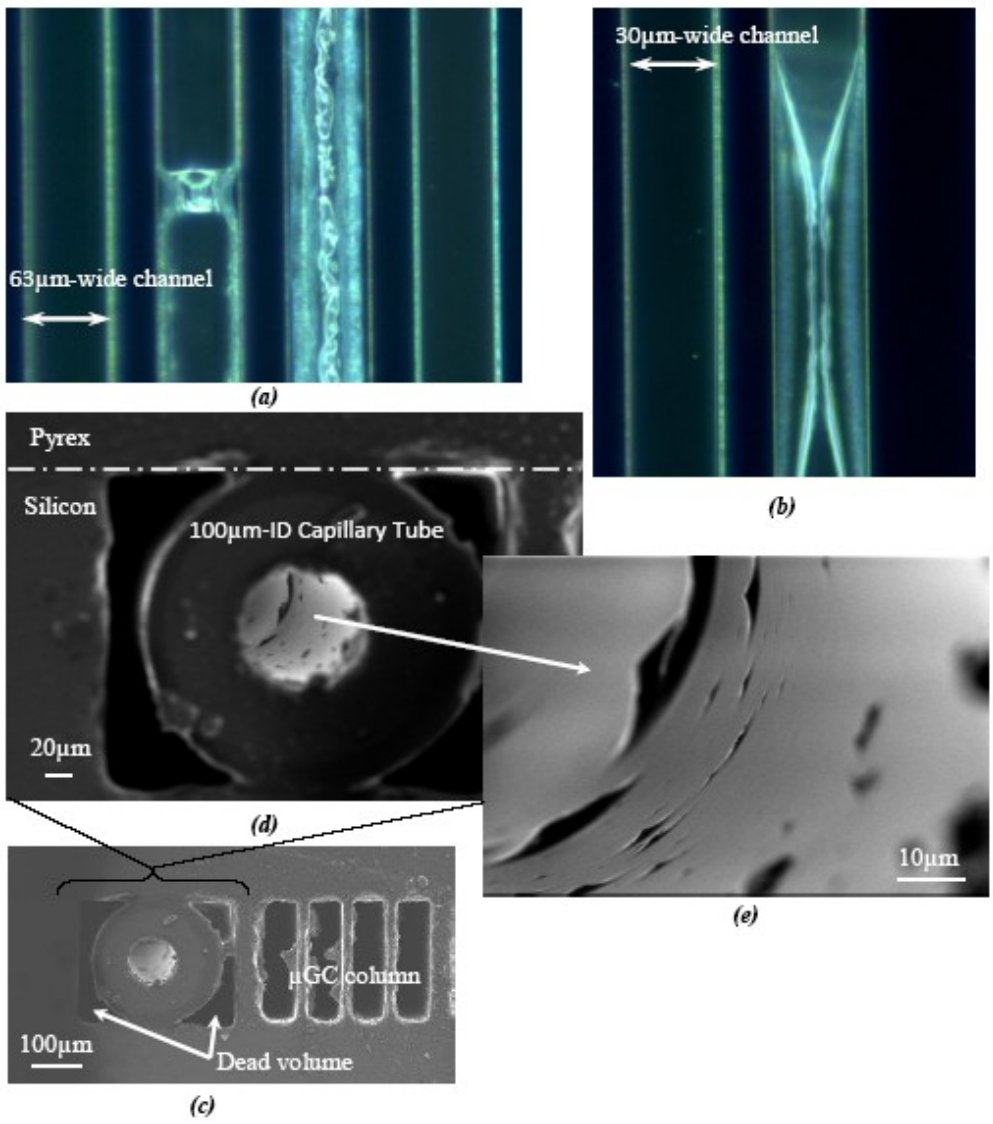

Figure 3.1 Conventional coating method and common problems, (a-b) optical images of µGC columns coated by static method show the plugged channels occurred during solvent evaporation, (c-d) SEM images from the inlet/outlet gate where the capillary tube is connected to the square-cross-section µGC column in order to transmit the coating solution into the column, the dead volumes created by the geometric change causes bubble generation during static coating, (e) thinning and thickening of coating layer causes low separation performance and large band broadening.

the efficiency of chip-based capillary electrophoresis [69]. Synovec's group reported dodecanethiol gold nanoparticles deposited on the inner surface of bare fused silica 100µm-ID capillary column [67]. In a more recent report, octadecylamine-capped gold

nanoparticles were used to coat the capillary column [61]. These techniques still have not been widely used due to tedious coating process to get stable coating, non-conformal and poor surface coverage of the column by nanoparticles and finally irreproducible retention time related to washing-off of nanoparticles over injections [68, 73]. Furthermore, carbon nanotubes (CNTs) have been reported as a new class of GC stationary phases [70, 71]. Their performance has been evaluated by depositing only on the bottom surface of the square cross-section of microfabricated channels due to the fabrication difficulties of depositing CNTs on all four sides of the channel [71].

The presented technique in this chapter shifts the coating procedure to the step before channel sealing and produces stationary phases with high uniformity, reproducibility, and robustness by merging microfabrication and nanotechnology. The columns are first coated by a thin layer of gold using seedless electroplating and then functionalized to tailor the surface properties for the separation of target compounds. The following sections describe the proposed fabrication steps and separation performance of the DRIE silicon-glass columns coated with monolayer-protected-gold (MPG).

3.2 Fabrication

The proposed fabrication method for μGC columns includes two major steps. First, the column configuration is fabricated by anisotropic etching of silicon to create serpentine channels. The second step is a novel surface treatment method to adjust the chemical properties of the channel surface and to enhance the separation capability of the column. The technical details of these two steps are explained in the following subsections.

3.2.1 Column Fabrication

In order to evaluate the proposed coating method, SCC columns with capillary widths ranging from 25μm to 100μm as well as MCCs comprising four 63μm-wide capillaries were designed and fabricated. All the columns had a length of 25cm. The fabrication of both silicon-glass SCCs and MCCs started with cleaning a silicon wafer in a Piranha solution. Then, an 8μm-thick layer of AZ9260 photoresist was spun on the wafer at 3k rpm for 60 seconds. After patterning the photoresist, the wafer was etched to a depth of

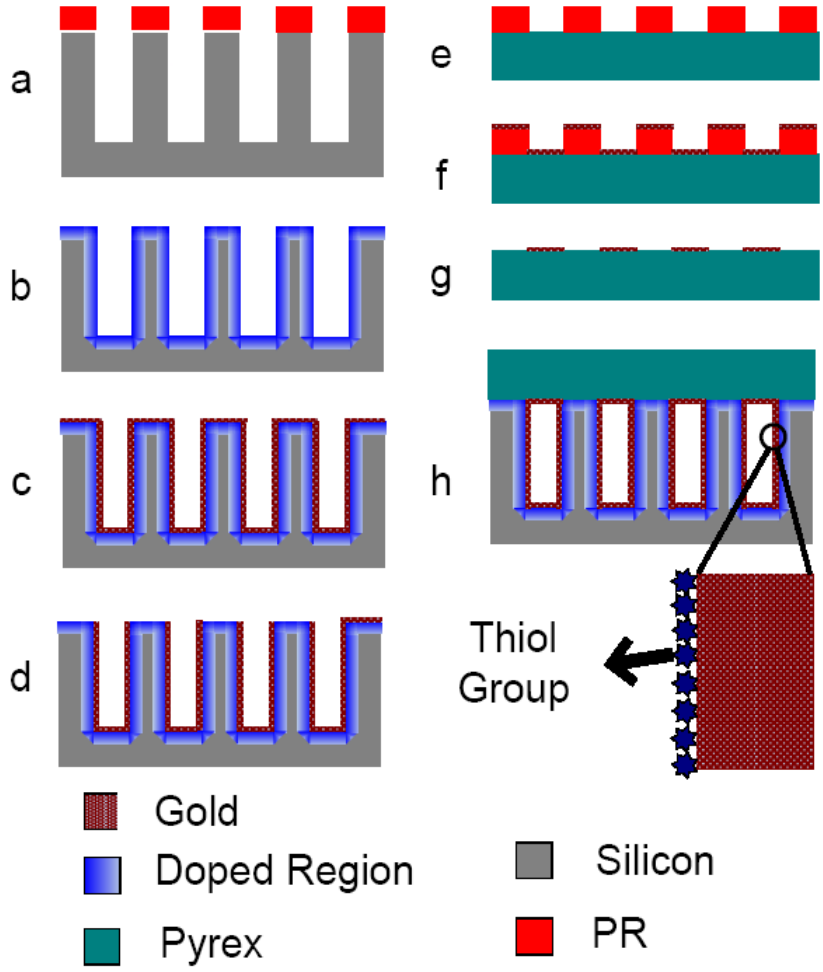

Figure 3.2 Fabrication process flow of the MEMS µGC column, (a) photolithography and anisotropic etching using DRIE, (b) phosphorous diffusion (c) seedless gold electroplating, (d) gold patterning by pulling the plated layer off from the top flat surface , (e-g) Ti/Au deposition and lift-off patterning on Pyrex wafer (h) anodic bonding of silicon and Pyrex wafer.

250µm using DRIE to form channels with aspect ratios varying between 1 (for 250µm-wide columns) and 10 (for 25µm-wide columns) (Figure 3.2a) [29]. In order to pattern the Pyrex wafer, a 1.5µm-thick layer of S-1813 photoresist was spun on the Pyrex at 2k rpm for 35 seconds. After developing the photoresist in MF-319, the desired thickness of Ti/Gold was deposited using Physical Vapor Deposition, PVD. Finally, the coated Pyrex

wafer was submerged in the acetone ultrasonic bath for 1hr to lift off the extra gold and release the pattern (Figure 3.2e-g).

3.2.2 Coating Method

The goal of this step is to deposit a uniform stationary phase layer on the column walls. An ideal stationary phase for μGC should exhibit selectivity and differential solubility of components to be separated and a wide operating temperature range. A phase should be chemically stable and have low vapor pressure at evaluated column temperatures. In order to achieve a stationary phase with these features while having a low cost and high yield process, we have developed a novel surface treatment which includes four steps: deposition, patterning, stabilization, and functionalizing.

3.2.2.1 Deposition

The uniform deposition thickness of the stationary phase has been a perpetual struggle. The film should have a constant thickness undisturbed by the corner of the rectangular channels or alternating thicker and thinner parts resembling waves. This task is much more challenging for ultra narrow μGC columns with high aspect ratios and sharp corners.

In order to overcome these challenges, for the first time in μGC development history, we used pulse electroplating technique to deposit a thin and conformal layer of gold directly on a heavily phosphorous doped (n^+) silicon wafer. This seedless electroplating provides a gold layer, which is chemically and thermally stable due to intrinsic gold properties and is easily patterned after deposition due to the weak adhesion between gold and silicon. Furthermore, the layer thickness is adjustable by varying the electroplating time to achieve the optimum separation performance of different column dimensions. Also, this gold layer covers all the active bonds of the silicon surface and eliminates the necessity of the deactivation process in conventional coating methods [29, 46, 74].

In order to begin the deposition process, the silicon wafer with etched channels is doped by solid source diffusion of phosphorous at 950^{o}C for 6 hours. The 2μm-deep doped region created on the silicon surface is used as the cathode. Furthermore, the residual of passivation polymer deposited on channel surface during the etch process

would be decomposed in the doping furnace ensuring the cleanliness of the silicon surface. Before dipping the channels in electroplating bath, the native oxide is etched by buffered hydrofluoric acid (BHF) for one minute. The electroplating bath is maintained at 55^{o}C with a stirring rate of 200rpm to provide a uniform distribution of gold ions in the bath. We used an acidic gold electroplating solution (TG-25 RTU, Technic Inc., USA) and a platinized Ti grid as the anode. The anode is placed at a distance of 2cm from the cathode and has a size at least two times larger than that of the cathode to afford a uniform electric field on the silicon wafer. The current between the platinized Ti grid anode and doped silicon cathode is controlled by a current square-pulse generator with the duration of τ and the period of *T*.

This current is supposed to be carried by gold ions which have a molar concentration of C_b inside the plating bath. The reduction of gold ions during electroplating reduces the ion concentration inside the etched channels to:

$$C_{ch} = [1 - \alpha(\tau, J, h, w)]C_b \tag{3.1}$$

where *c, J, h* and *w* are correction factor, electroplating current density, depth and width of the channels, respectively. It has been shown that the smaller value of α results in a more uniform deposition [75]. Therefore, we need to determine α based on the experimental parameters to optimize plating conditions and enhance the deposition uniformity.

It is worth mentioning that α is also a function of the location inside the channels [75]. It gradually changes from the value of one at the plating zone near the channel surfaces to the value of zero far away from silicon wafer inside the plating bath. The theoretical model to describe this change is based on the Fick's second law for ion diffusion and is presented for one-dimension (flat surface) in [76]. However, to simplify the model applicable to our experiments without missing the concept we assume an average concentration inside the channel.

The reduction reaction ($Au^{z+} + ze^{-} \rightarrow Au$) consumes *z* (=1 for gold) electrons provided by the plating current. Therefore, the number of reduced gold ions, *n*, and plating current, *I*, are related according to the following equation:

$$q = I \cdot \tau = z \cdot e \cdot n \tag{3.2}$$

where e is the electron charge and q is the total charge transferred from the cathode to the electroplating solution. The number of reduced ions in a channel with depth of h, width of w, and length of l is determined by the ion concentration decrease:

$$n = N_A\,(hwl)(C_b - C_{ch}) \tag{3.3}$$

where N_A is Avogadro constant ($6.022 \times 10^{23}\ mol^{-1}$). From Eq. (3.1) to (3.3) and using current density, J, to calculate the plating current, the following equation is derived:

$$\alpha = \frac{J}{zFC_b}\frac{2h + w}{hw}\tau \tag{3.4}$$

where F is Faraday constant and is equal to eN_A=*96,487 C mol*$^{-1}$. Figure 3.3 shows the effect of J and α on the uniformity and quality of the deposited gold layer. A smaller J results in a smaller grain size and a smaller α yields more uniform coverage. Therefore, considering this fact and using equation (3.4), the values of τ and J have been adjusted to afford a value of about *.01* for α and to achieve uniform coverage all over the channel surfaces. For example, for *J=3 mA/cm*^{2}, C_b *=120 oz/gal* of sodium gold sulfite, *h=250μm*, *w=25μm* and τ = 1sec, α would be *.012.*

The above mentioned model assumes that the ion concentration is built up to C_b during relaxation time (T-τ , while plating current is zero). Therefore, relaxation time should be greater than the required time for gold ions to diffuse from the electroplating bath to the channels and build up the concentration from C_{ch} to C_b. We hypothesize that diffusion is the dominant ion transport due to the negligible stirring effect inside these narrow deep channels. The current due to this charge transport is[76]:

$$i = zFD\frac{\partial C}{\partial x} \tag{3.5}$$

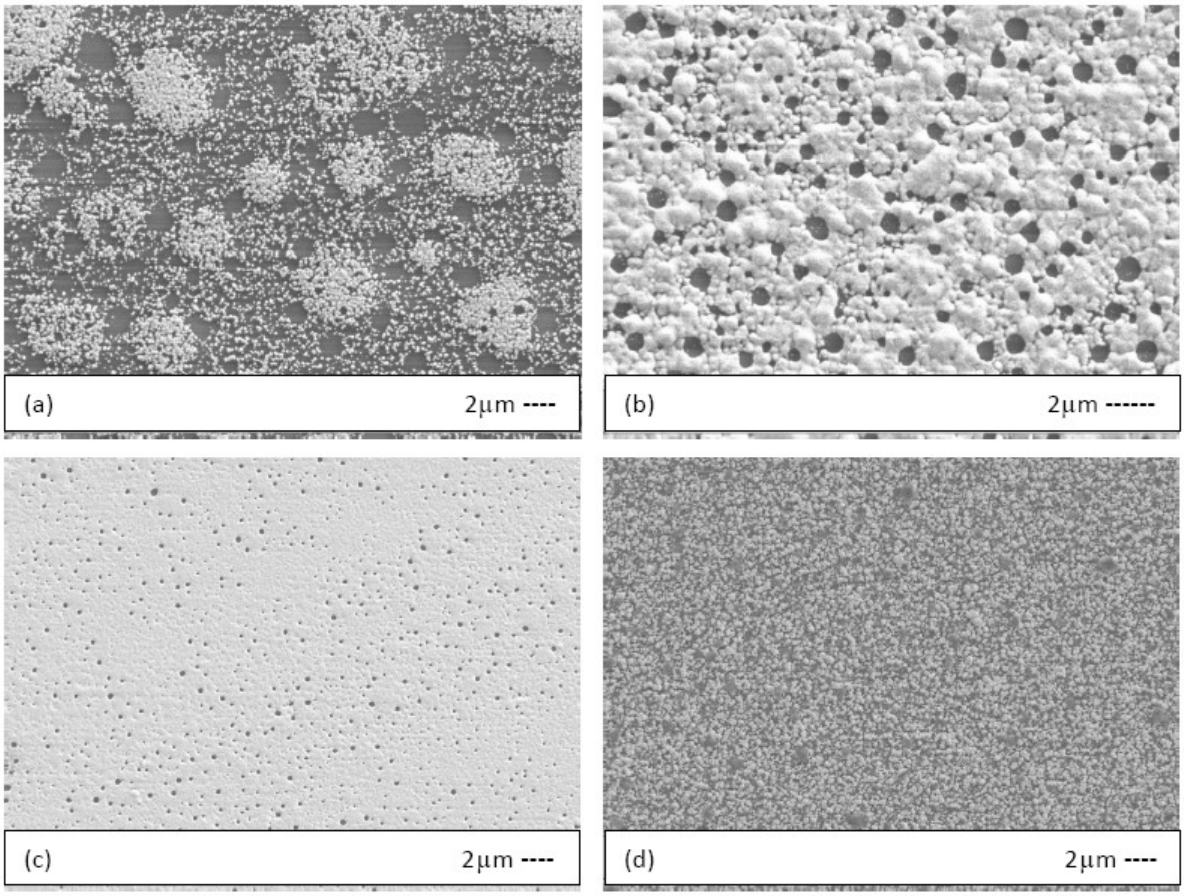

Figure 3.3 SEM images show the effect of current density, J, and correction factor, α, on deposition quality (a) poor coverage for J=3mA/cm2 and α=0.7, (b) reticulated coverage for J=3mA/cm2 and α=0.4, (c) good overage with small grain for J=3mA/cm2 and α=0.1, (d) good overage with large grain for J=8mA/cm^2 and α=0.1.

where D is the diffusion coefficient and x is the normal direction to the flat silicon surface. The minimum required relaxation time, t_{min}, is the time required to increase the ion concentration, C, from C_{ch} to C_b. Assuming C as a linear function with the value of zero near the silicon surface, the average diffusion current during build up time is:

$$\bar{\imath} = zFD\frac{C_b}{h} \tag{3.6}$$

The total charge transferred by the buildup average current is equal to the total charge transferred by the plating current, thus by using equation (3.2):

Table 3-1 Deposited gold layer thickness v.s. different electroplating condition.

Case No.	J (mA/cm^2)	T (s)	τ (ms)	α	Plating time (min)	Transferred Charge (mC/cm^2)	Average Thickness (nm)	Standard Deviation (%)
1	4	60	1000	.016	60	240	247	5.5
2	6	60	1000	.024	60	360	350	2.2
3	6	6	100	.002	60	360	361	3.4
4	6	6	100	.002	30	180	180	2.4
5	6	6	100	.002	90	540	540	3.7

$$q = \bar{\imath} t_{min} = J\tau \qquad (3.7)$$

Finally by plugging equation (3.4) into equation (3.7):

$$t_{min} = \alpha \frac{1}{D} \frac{\mathrm{wh}}{2 + {}^{w}/_{h}} \leq \mathrm{T} - \tau \qquad (3.8)$$

As the above equation shows, the pulse period should increase by increasing the cross-section area (*hw*) or aspect ratio (*h/w*). We adjust the time period for all the experiments to satisfy the above condition.

As mentioned earlier, the stationary phase thickness should be adjusted based on the column dimensions to achieve maximum separation performance. Therefore, the deposited thickness of gold layer has been characterized for different electroplating conditions (current density and pulse shape). Table 3-1 shows electroplating parameters to deposit a thickness varied from 180nm to 540nm suitable for all the column dimensions designed in this work.

3.2.2.2 Patterning

In order to seal the etched channels in silicon by a Pyrex substrate using anodic bonding, the gold layer on the top flat surface should be removed. As Figure 3.4 shows, the seedless electroplated gold has very low but adequate adhesion to silicon. This is a

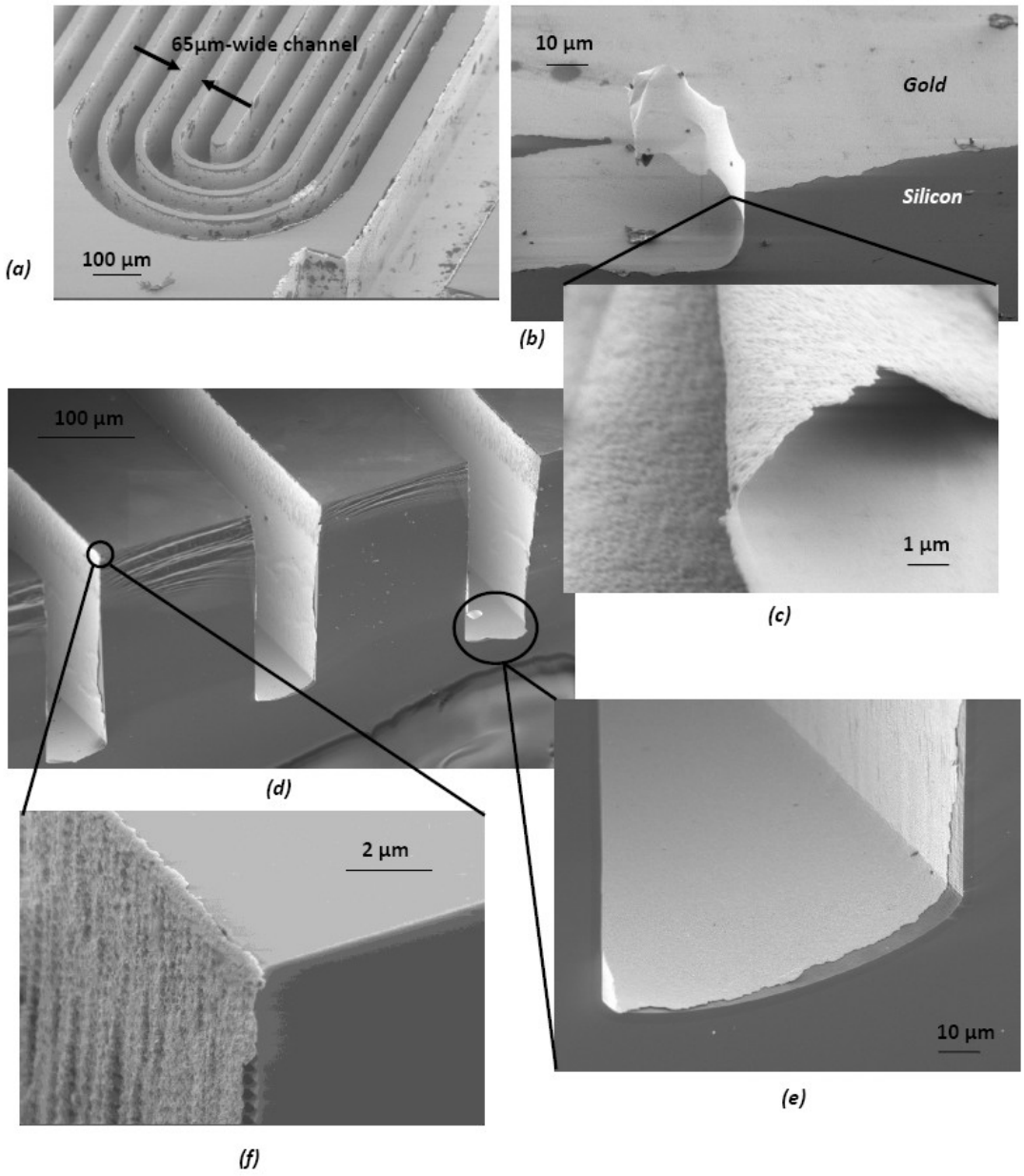

Figure 3.4 SEM images show the deposition quality, (a) 4-channel MCC after removing gold from the top flat surface, (b) gold layer folded by mechanical force demonstrating its low adhesion, (c) cross-section of 150nm-thick gold layer showing the uniformity of plated layer, (d-f) broken column after polishing the top flat surface showing the gold coverage on the walls and corners with a uniform thickness .

critical characteristic making it easily removable from the top flat surface by an adhesive tape without affecting the coverage on the column sidewalls (Figure 3.5). Furthermore,

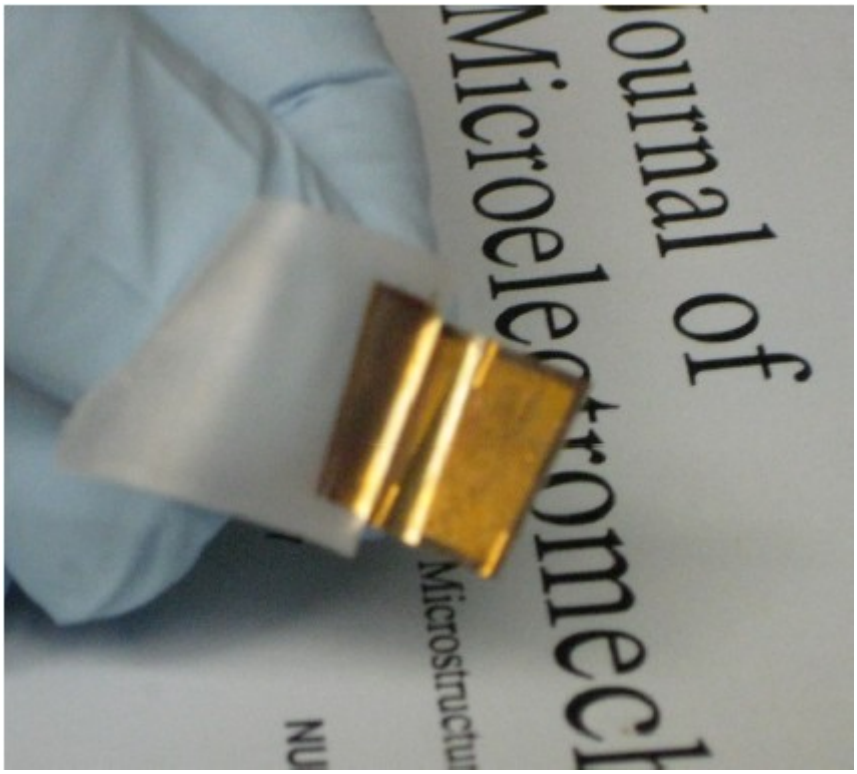

Figure 3.5 Optical image shows the fabrication step for removing gold from top flat surface using adhesive tape.

the high value of silicon Young's modulus causes its perseverance to high vertical stress. This clearly demonstrates that it is possible to pattern the gold layer even for very tiny structures without applying any shear stress. After this patterning step, the silicon wafer was anodically bonded to the Pyrex 7740 substrate patterned with evaporated Ti/Au. The bonding temperature and pressure were 350^{o}C and 2KPa, respectively. Applying a DC voltage of 1250V for 20 minutes established a permanent bond. Figure 3.6 shows optical images of the μGC column before and after polishing the gold from top-flat surface and also the released column after bonding.

3.2.2.3 Stabilization

Thermal annealing during the bonding process at temperatures less than the Si-Au eutectic temperature (365^{o}C) stabilizes the electroplated gold by significantly improving

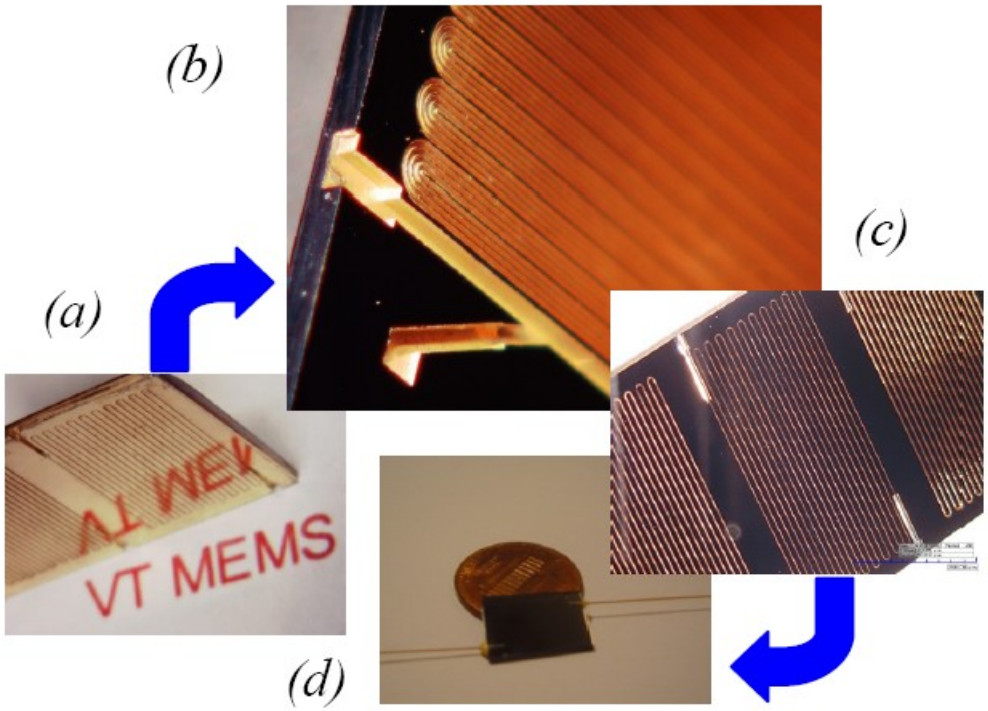

Figure 3.6 optical images show deposition and patterning steps, (a) 25µm-wide, 25cm-long, 250µm-deep SCC coated by 150nm gold layer; the reflective surface shows the quality of the deposition (b) 4-channel MCC after gold patterning (c) 25µm- and 100µm wide SCCs after gold plating (d) a µGC column die.

its adhesion to the doped silicon surface [77]. The gold coating was proved to be stable under GC operating temperature (350^{o}C) and flow conditions (1ml/min). After bonding, the wafer was diced and fused silica capillary tubing with 167-µm-O.D. and 100-µm-I.D. was attached to fluidic ports using epoxy (epoxy907, Miller-Stephenson Co., US).

3.2.2.4 Functionalizing

The last step is performed by filling the column with a solution of octadecylthiol ($C_{18}H_{35}SH$) in hexane for six hours. This functionalizing process attached the alkane group to the electroplated gold surface by self assembly (SAM) and resulted in a monolayer-protected gold (MPG) layer that could be used as a stationary phase [78]:

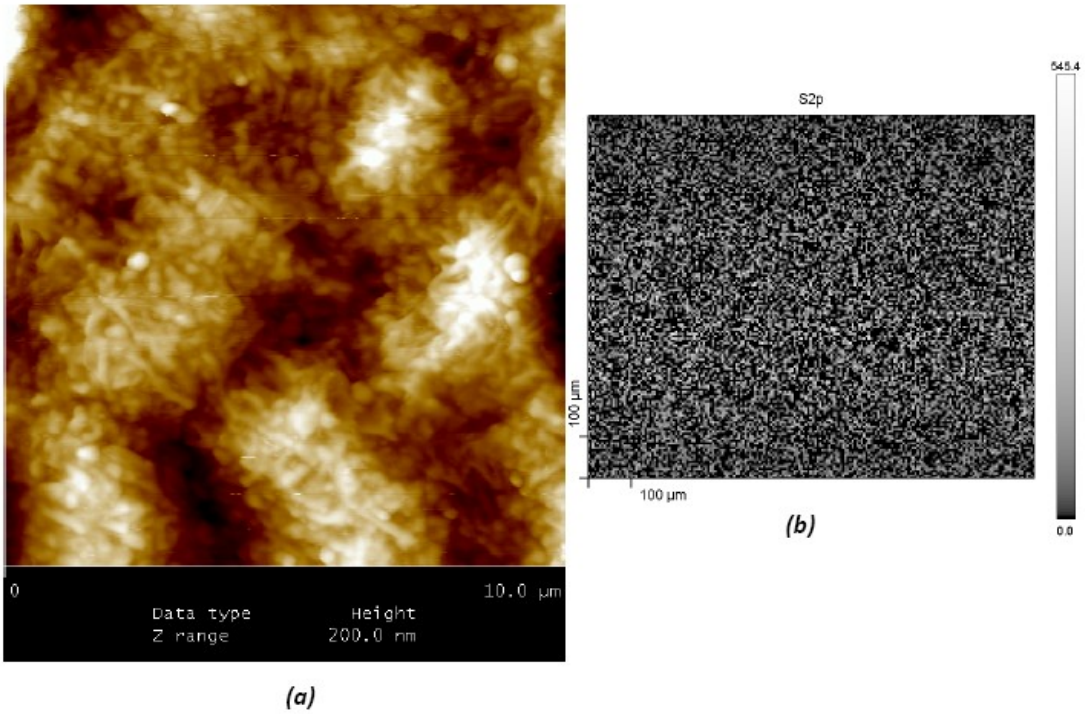

Figure 3.7 Surface Analysis, (a) AFM image shows the topology of the 200nm-thick pulse electroplated gold (b) SIMS image of MPG coated silicon surface shows the existence and uniformity of the sulfur (white dots)

$$C_{18}H_{35}SH + Au^0 \xrightarrow{SAM} [C_{18}H_{35}S^- + Au^+] + {}^1/_2\, H_2 \tag{3.9}$$

The formation of gold SAMs permits a variety of functional groups to be incorporated into the monolayer, providing a versatile route to the formation of different surface properties for different µGC applications [67, 79].

Figure 3.7a and Figure 3.8 show an AFM image and SEM images of the gold surface topology and its nanometer-scale grain size. The secondary ion mass spectrometry (SIMS) analysis, Figure 3.7b, proves the existence and the high uniformity of sulfur (thiol monolayer) on a 100µm square area of the gold surface.

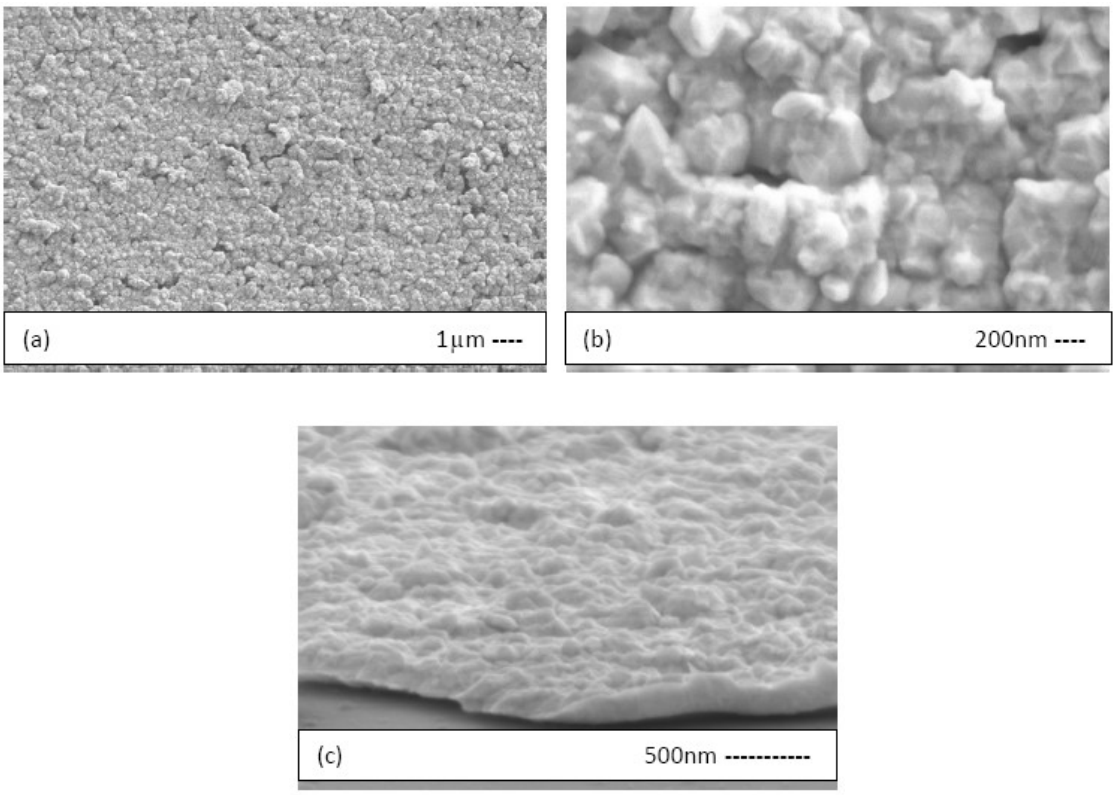

Figure 3.8 SEM images shows the surface topology of the 250nm-thick gold layer deposited by 4mA/cm2 current density (case1, Table 1), (a-b) top view with different magnifications, (c) side view

3.3 Experiments and Results

In order to evaluate the capabilities of the microfabricated columns, several experiments were conducted using conventional GC system (5890 Series II GC, Hewlett Packard) having a split inlet (200:1) and flame ionization detector (FID). The capillary column inside the GC was replaced by the MEMS column. The autosampler (7673B, Hewlett Packard) was used to inject the samples. Air was used as a carrier gas. All gases were purified with filters for water vapor and hydrocarbons. The injector and FID temperatures were both maintained at 280^{o}C.

The efficiency of GC columns is expressed by the height-equivalent-to-a-theoretical-plate (*HETP*). Dodecane was used to determine *HETP* because of having a retention

factor greater than 10, thus making *HETP* less dependent on the compound selected (k) and experimental conditions (mainly temperature) [30].

HETP was measured by injecting a 1µL mixture of dodecane ($C_{12}H_{20}$) and methylene chloride (CH_2Cl_2). The dodecane retention time t_R was used to determine the *HETP* experimentally based on:

$$HETP = \frac{L}{5.54\left(\frac{t_R}{w_h}\right)^2} = \frac{1}{Plate\ Number} \tag{3.10}$$

where L and w_h are the length and width of the peak at the half height. Only symmetric peaks (symmetry of 0.9-1.1) were used to measure *HETP*.

Table 3-2 shows the experimental measurements of plate number for single-capillary (SCC) and multi-capillary (MCC) columns with different channel widths. 25µm-wide columns with the MPG stationary phase have yielded 20,000 plates/m. In addition, this is the first time that we have been able to successfully coat MEMS-based MCCs to achieve high-performance separations of concentrated samples. Furthermore, the separation performance of the SCCs and MCCs have been explored by separating a gas mixture containing n-alkanes (C_9-C_{10}-C_{12}-C_{14}-C_{16}) (Sigma-Aldrich Inc., MO, US), in the conventional GC oven. Figure 3.9 shows the gas separations obtained by the high performance ultra-narrow columns (25µm-wide SCCs) and high sample capacity columns (4-channel MCCs with 65µm-wide capillaries) at a 30^{o}C/min temperature programming rate in less than three minutes. It is worth mentioning that the sample concentration in MCC case is almost ten times more than the sample used for SCC to show the higher sample capacity of MCC design. The SCC column was saturated at this sample concentration and could not produce any separation. In order to compare the performance of MPG and conventional phases, a 250µm-ID commercially coated column (RXI-1ms, Restek Co.) by PDMS phase has been selected and evaluated at the same chromatographic conditions. To have a fair comparison, a length of 125cm of this column separated from the original 15m-long column affording the same plate number (5000) as the 25cm-long 25µm-wide SCCs in Figure 3.9. Figure 3.10 shows the separation chromatogram obtained from this column at a 30^{o}C/min programming rate and 1psi inlet

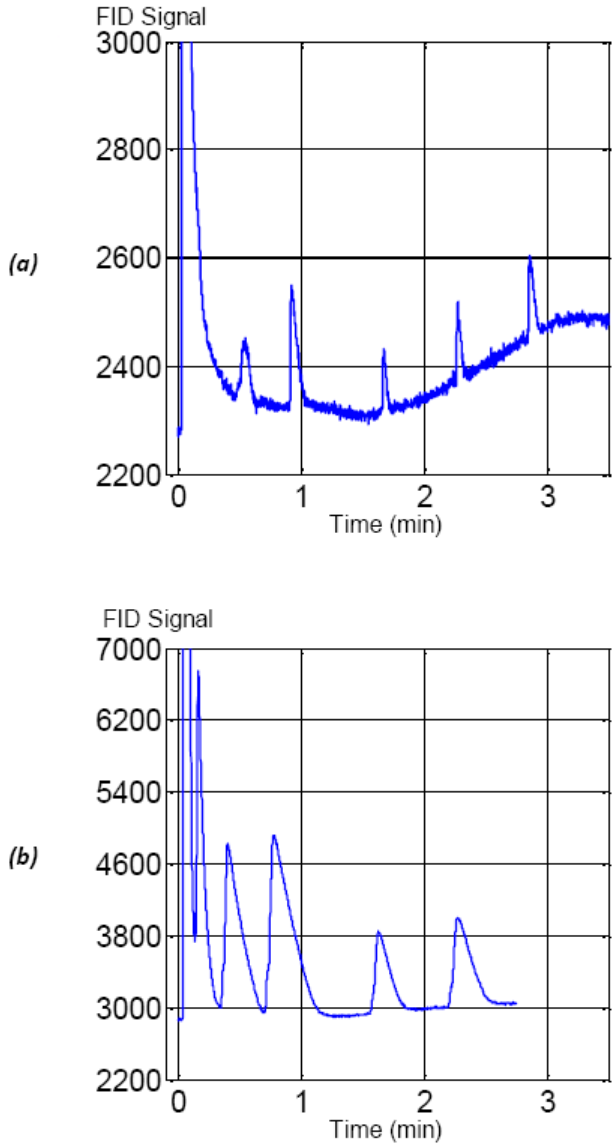

Figure 3.9 Chromatogram of five alkanes (in order from left to right C9, C10, C12, C14, C16), obtained by 25µm-wide SCC (top) and 4-capillary MCC (bottom) at temperature rate of 30oC/min.

pressure. The small length of the column causes fast elution of nonane and decane in less than 30sec even when the minimum possible inlet pressure was used. The comparison between Figure 3.10 and Figure 3.9a for the rest of the alkanes (C_{12}-C_{14}-C_{16}) shows approximately similar performance in terms of band broadening and retention time.

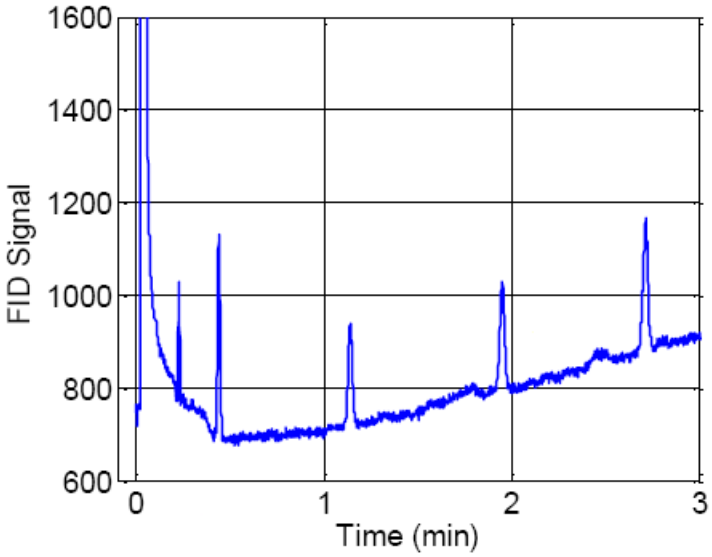

Figure 3.10 Commercial column performance, GC chromatogram of n-alkanes (in order from left to right C9, C10, C12, C14, C16) obtained at a temperature rate of 30oC/min and 1psi inlet pressure showing the separation performance of125cm-long 250µm-ID commercially coated column (RXI-1ms, Restek Co.) having the same plate number(5000) as the 25µm-wide 25cm-long MPG coated µGC column.

Figure 3.11a illustrates the analysis time stability of MPG stationary phase. The retention time variation is less than 10% which could also be related to the experiment conditions. The stationary phase reproducibility is shown in Fig. 11b which is a separation chromatogram of four polar alcohol (*Pentanol, Hexanol, Heptanol and Octanol*) obtained at a temperature rate of 50^{o}C/min and 30 psi inlet pressure.

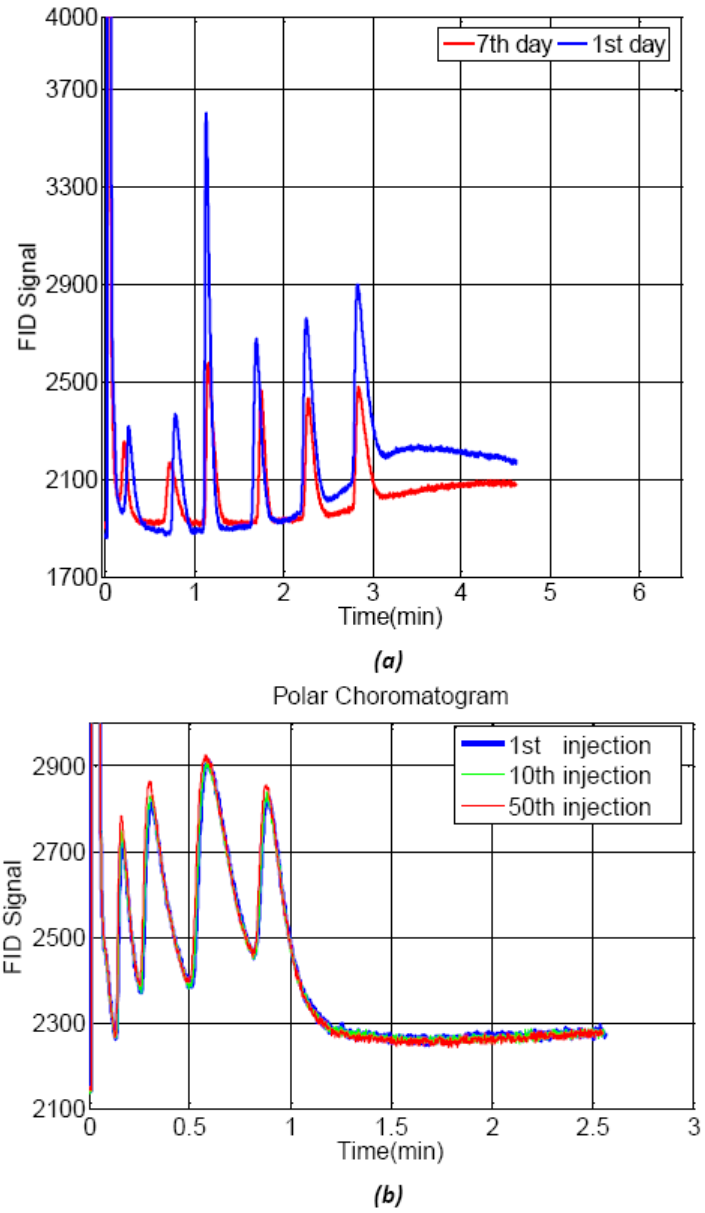

Figure 3.11 Time stability and reproducibility of MPG stationary phase, (a) GC chromatograms of n-alkanes (in order from left to right C8, C9, C10, C12, C14, C16) obtained at a temperature rate of 50oC/min and 30psi inlet pressure showing the MPG coating stability over a time period of seven days, (b) GC chromatograms ofpolar alcohols (Pentanol, Hexanol, Heptanol and Octanol) obtained at a temperature rate of 50°C/min and 30psi inlet pressure showing the excellent coating robustness

The column bleed, as the last characterization factor evaluated in this report, is the loss of stationary phase pieces which are either the result of impurities in the stationary

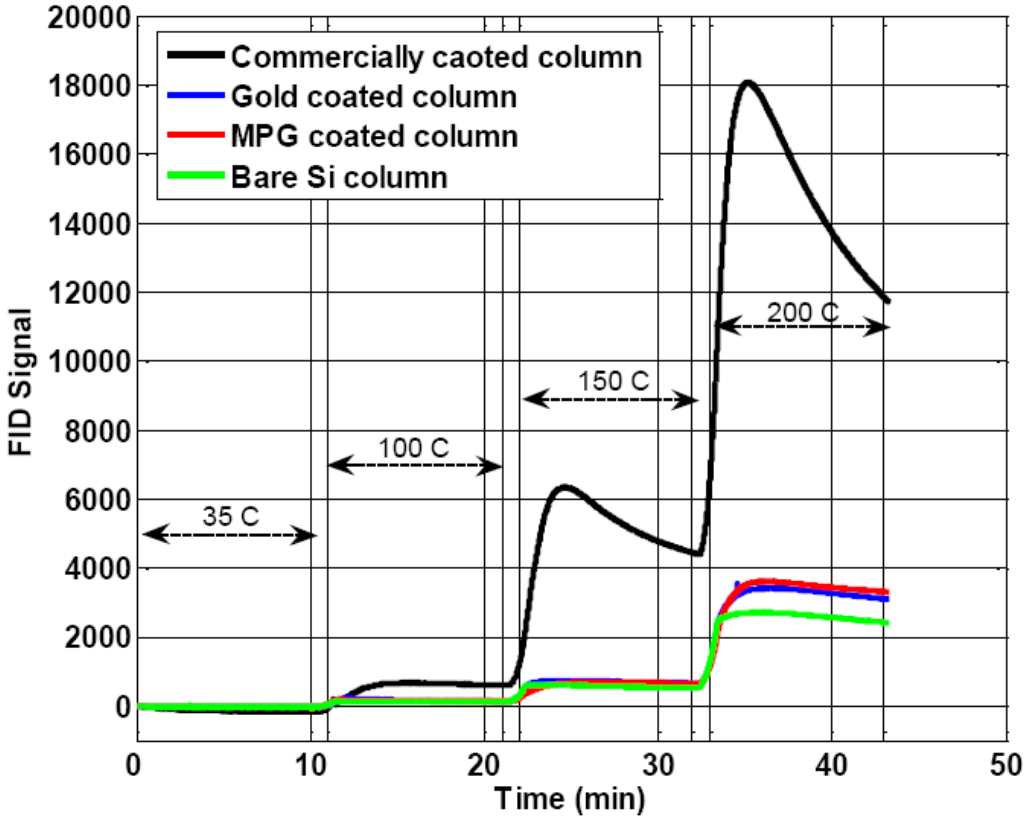

Figure 3.12 Column bleed comparison between (1) 125cm-long 250µm-ID commercially coated column (RXI-1ms, Restek Co.), (2) 250µm-wide 25cm-long µGC column (3) the same column in (2) coated by 300nm-thick electrodeposited gold, (4) the same column in (3) after functionalizing with octadecylthiol, experiment conditions: constant flow of 2.2 sccm of nitrogen, oven program: 35°C for 10min to 100 °C @ 50 °C/min for 10min to 150 °C @ 50 °C/min for 10min to 200 °C @ 50 °C/min for 10min.The values presented here are after three times conditioning under the mentioned oven program.

phase or the decomposition of the phase at elevated temperatures. Column bleed can also be an indicator of the stability and lifetime. When using sensitive detectors such as a mass spectrometer, bleed can impact the detection limits and cause difficulties at the low calibration range [8]. In order to estimate the MPG coated column bleed, the 250µm-wide 250µm-deep 25cm-long µGC columns were evaluated under a constant nitrogen flow of 2.2sccm at four different temperatures of 35°C, 100°C, 150°C and 200°C. The temperatures were kept constant for 10min for each experiment. The temperature ramp of 50°C/min used to increase the oven temperature between each two set points. This

Table 3-2 Experimental results, shows the column performance evaluated by measuring plate number (N), using dodecane (retention factor, k>10) at 65oC isothermal chromatogram.

Column Design	***Plate number MPG***
100µm-SCC	**3000**
25µm-SCC	**20000**
4-MCC	**7700**

experiment was done at least three times for µGC columns with three different surface properties: 1) without any coating 2) coated with a 300nm-thick electrodeposited gold layer, and 3) coated with 300nm-thick electrodeposited gold and functionalized by the octadecylthiol monolayer. Furthermore, 250µm-ID 125cm-long commercially coated capillary column was tested under the same experimental conditions. Figure 3.12 shows the FID signal obtained from the column bleed test. The difference between the signal obtained from bare silicon column and the one obtained from MPG coated column stems from stationary phase bleed. As Figure 3.12 shows, the MPG bleed is almost negligible (at least one order of magnitude smaller) compared to the commercially coated column. The bare silicon column bleed is mostly related to the decomposition of polymer-based epoxy used to connect the capillary tube to the µGC column. This statement has been proved by bleed testing of two exact similar columns in stage (1) with two different adhesive glues (epoxy907, Miller-Stephenson Co., US and epoxy118-15A/B, Creativematerials, US). The resulted FID signals had significantly different values showing the effect of the adhesive glue on the column bleed. It is worth mentioning that in an integrated µGC system, column, detector and heaters are on a single chip and there is no need to use capillary connectors.

3.4 Conclusion

One critical advantage of the MEMS-based silicon-glass µGC column fabrication exploited in this research is the accessibility of the inner surfaces of the column prior to anodic bonding. This paper reports for the first time a high-yield MEMS-based surface

treatment method for high-aspect ratio μGC separation channels. This new stationary phase coating technique is based on seedless gold electroplating on the etched silicon and PVD gold deposition on the flat Pyrex prior to anodically bonding and then functionalizing the gold layer with thiol groups using self assembly subsequent to anodically bonding. The conformal deposition of gold with varying thickness, ability to be patterned on 3D structures and eliminating the formation of thicker regions at the corners are the main advantage of this method. Furthermore, the inherent properties of gold such as biocompatibility, conductivity and chemical stability are another important feature of the technique presented in this paper. It is notable that a wide variety of thiol-based organic molecules can be self-assembled to tune the polarity of this new class of μGC stationary phases.

4 Future Work

According to the author's experience and knowledge the future of the μGC column development, especially the one presented in this work, is organized into three main directions.

4.1 Self-Patterned Electrodeposition

The first suggested research direction is the experimental and theoretical evaluation of an unknown phenomenon discovered in this work and named self-patterned seedless gold electroplating [to be presented in Transducer09]. For a specific channel design and electroplating pulse shape, electrodeposition occurs only on the vertical surfaces and not on the horizontal surfaces. Figure 4.1 shows the SEM images from conformal and self-patterned electrodeposited gold. The ability to cover only vertical surfaces of three dimensional (3D) structures is a significant achievement in microsystems technology serving a wide range of applications including gas chromatography (GC). Furthermore, the fabrication process proposed in Chapter 3 would be simplified by removing the patterning step. Therefore the presented surface treatment could be applied for ultra-tiny structures which are not stable under mechanical stress during the patterning step.

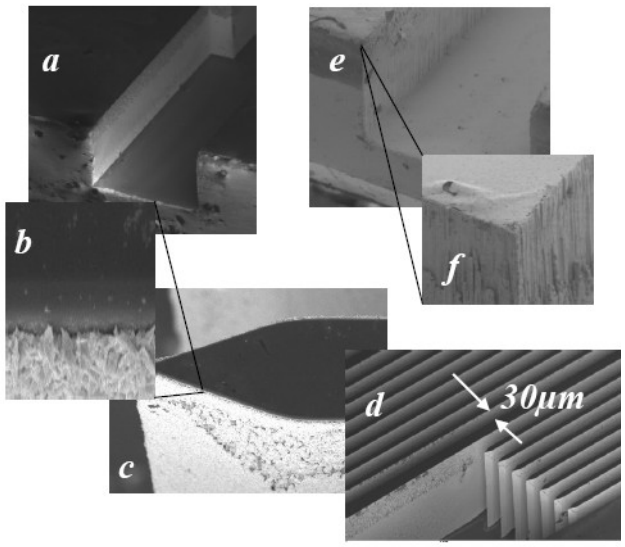

Figure 4.1 SEM images of 250μm-deep channels show the deposition quality, (a-d) self-patterned electroplated gold only on the vertical surfaces. (e-f) conformal plated gold covers vertical, horizontal and edges.

In order to scientifically study this phenomenon, it is suggested that the plating current and voltage wave be monitored during electrodeposition using a high-sampling-

rate oscilloscope. These waves should be analyzed using a frequency spectrometer to determine the effect of the high frequency harmonics. Furthermore, the effect of the pulse shape and channel design should be evaluated. The required mask has been designed with different channel width (30μm and 150μm) and channel spacing (25μm and 100μm).

4.2 Gold: The First Conductive Stationary Phase

The second proposed research approach is based on the conductive nature of gold. This feature would have two applications: 1) The deposited stationary phase can be used as the heater to decrease the power consumption of the temperature programming, afford higher temperature ramp, and simplify the fabrication process. This self-heating feature could also be used in pre-concentration devices due to the ultra-fast heating and ultra-sharp released-peaks [submitted to IEEE Sensor09]. 2) This conductive stationary phase could be used as an electrode to create an electric field inside the μGC column. The resultant electric field would trap the polar molecules to enhance the concentration factor of the pre-concentration devices. Furthermore, it can be used to affect the retention time of molecules in a GC column. A microwave/RF electric field may show heating effects as well.

4.3 Gold and Its Inherent Properties

Pure gold and treated gold have not been widely used as stationary phase in gas sensors. Therefore most of their separation/adsorption properties are not discovered. For example, our experiments showed for the first time that gold can be a selective adsorbent for polar components in pre-concentration devices [submitted to EMBC 09]. Furthermore, there is a wide range of self-assembled layers which can be used to treat the gold surface properties and enhance its separation/adsorption properties. This research direction mostly focused on the chemical side of the separation devices.

References

[1] I. Phenomenex, "Zebron ZB-XLB," http://phenomenex.com, 2009.

[2] B. E. S. Group, "Gas Chromatography-Mass Spectrometer

(Thermo-Finnigan)," http://besg.group.shef.ac.uk, 2009.

[3] S. C. Terry, J. H. Jerman, and J. B. Angell, "A gas chromatographic air analyzer fabricated on a silicon wafer," *Electron Devices, IEEE Transactions on,* vol. 26, pp. 1880-1886, 1979.

[4] M. Agah and K. D. Wise, "Low-mass PECVD oxynitride gas chromatographic columns," *Microelectromechanical Systems, Journal of,* vol. 16, pp. 853-860, 2007.

[5] M. Agah, J. A. Potkay, G. Lambertus, R. Sacks, and K. D. Wise, "High-performance temperature-programmed microfabricated gas chromatography columns," *Microelectromechanical Systems, Journal of,* vol. 14, pp. 1039-1050, 2005.

[6] E. S. Kolesar, Jr. and R. R. Reston, "Review and summary of a silicon micromachined gas chromatography system," *Components, Packaging, and Manufacturing Technology, Part B: Advanced Packaging, IEEE Transactions on,* vol. 21, pp. 324-328, 1998.

[7] P. R. Lewis, P. Manginell, D. R. Adkins, R. J. Kottenstette, D. R. Wheeler, S. S. Sokolowski, D. E. Trudell, J. E. Byrnes, M. Okandan, J. M. Bauer, R. G. Manley, and C. Frye-Mason, "Recent advancements in the gas-phase MicroChemLab," *Sensors Journal, IEEE,* vol. 6, pp. 784-795, 2006.

[8] R. L. Grob and E. F. Barry, *Modern practice of gas chromatpgraphy*, fourth ed. Hoboken: John Wiley & Sons, 2004.

[9] J. A. Potkay, G. R. Lambertus, R. D. Sacks, and K. D. Wise, "A Low-Power Pressure- and Temperature-Programmable Micro Gas Chromatography Column," *Microelectromechanical Systems, Journal of,* vol. 16, pp. 1071-1079, 2007.

[10] E. S. Kolesar, Jr. and R. R. Reston, "Silicon-micromachined gas chromatography system used to separate and detect ammonia and nitrogen dioxide. II. Evaluation, analysis, and theoretical modeling of the gas chromatography system," *Microelectromechanical Systems, Journal of,* vol. 3, pp. 147-154, 1994.

[11] N. Hong-seok, P. J. Hesketh, and G. C. Frye-Mason, "Parylene gas chromatographic column for rapid thermal cycling," *Microelectromechanical Systems, Journal of,* vol. 11, pp. 718-725, 2002.

[12] A. Bhushan, D. Yemane, E. B. Overton, J. Goettert, and M. C. Murphy, "Fabrication and Preliminary Results for LiGA Fabricated Nickel Micro Gas Chromatograph Columns," *Microelectromechanical Systems, Journal of,* vol. 16, pp. 383-393, 2007.

[13] M. Agah, G. R. Lambertus, R. Sacks, and K. Wise, "High-Speed MEMS-Based Gas Chromatography," *Microelectromechanical Systems, Journal of,* vol. 15, pp. 1371-1378, 2006.

[14] J. H. Jerman and S. C. Terry, "A miniature gas chromatograph for atmospheric monitoring," *Environment International,* vol. 5, pp. 77-83, 1981.

[15] R. R. Reston and E. S. Kolesar, Jr., "Silicon-micromachined gas chromatography system used to separate and detect ammonia and nitrogen dioxide. I. Design, fabrication, and integration of the gas chromatography system," *Journal of Microelectromechanical Systems,* vol. 3, pp. 134-46, 1994.

[16] M. A. Zareian-Jahromi and M. Agah, "Micro Gas Chromatography Multicapillary Columns with Mono-Layer Protected Gold as a Stationary," in *22nd Annual IEEE Conference on Micro Electro Mechanical Systems* Italy, 2009, pp. 288-291.

[17] S. Zampolli, I. Elmi, J. Stürmann, S. Nicoletti, L. Dori, and G. C. Cardinali, "Selectivity enhancement of metal oxide gas sensors using a micromachined gas chromatographic column," *Sensors and Actuators B: Chemical,* vol. 105, pp. 400-406, 2005.

[18] R. A. Miller, E. G. Nazarov, G. A. Eiceman, and A. Thomas King, "A MEMS radio-frequency ion mobility spectrometer for chemical vapor detection," *Sensors and Actuators A: Physical,* vol. 91, pp. 301-312, 2001.

[19] R. S. Chang Young Lee, Adarsh D. Radadia, Richard I. Masel, Michael S. Strano,, "On-Chip Micro Gas Chromatograph Enabled by a Noncovalently Functionalized Single-Walled Carbon Nanotube Sensor Array13," *Angewandte Chemie,* vol. 120, pp. 5096-5099, 2008.

[20] V. R. Reid and R. E. Synovec, "High-speed gas chromatography: The importance of instrumentation optimization and the elimination of extra-column band broadening," *Talanta,* vol. 76, pp. 703-717, 2008.

[21] A. Malainou, M. E. Vlachopoulou, R. Triantafyllopoulou, A. Tserepi, and S. Chatzandroulis, "The fabrication of a microcolumn for gas separation using poly(dimethylsiloxane) as the structural and functional material," *Journal of Micromechanics and Microengineering,* vol. 18, p. 105007 (6 pp.), 2008.

[22] S.-I. Ohira and K. Toda, "Micro gas analyzers for environmental and medical applications," *Analytica Chimica Acta,* vol. 619, pp. 143-156, 2008.

[23] C. J. Lu, W. H. Steinecker, W. C. Tian, M. C. Oborny, J. M. Nichols, M. Agah, J. A. Potkay, H. K. L. Chan, J. Driscoll, R. D. Sacks, K. D. Wise, S. W. Pang, and E. T. Zellers, "First-generation hybrid MEMS gas chromatograph," *Lab on a Chip,* vol. 5, pp. 1123-1131, 2005.

[24] K. Hanseup, W. H. Steinecker, S. Reidy, G. R. Lambertus, A. A. Astle, K. Najafi, E. T. Zellers, L. P. Bernal, P. D. Washabaugh, and K. D. Wise, "A Micropump-Driven High-Speed MEMS Gas Chromatography System," in *Solid-State Sensors, Actuators and Microsystems Conference, 2007. TRANSDUCERS 2007. International*, 2007, pp. 1505-1508.

[25] E. T. Zellers, S. Reidy, R. A. Veeneman, R. Gordenker, W. H. Steinecker, G. R. Lambertus, K. Hanseup, J. A. Potkay, M. P. Rowe, Z. Qiongyan, C. Avery, H. K. L. Chan, R. D. Sacks, K. Najafi, and K. D. Wise, "An Integrated Micro-Analytical System for Complex Vapor Mixtures," in *Solid-State Sensors, Actuators and Microsystems Conference, 2007. TRANSDUCERS 2007. International*, 2007, pp. 1491-1496.

[26] D. Cruz, J. P. Chang, S. K. Showalter, F. Gelbard, R. P. Manginell, and M. G. Blain, "Microfabricated thermal conductivity detector for the micro-ChemLab(TM)," *Sensors and Actuators B: Chemical,* vol. 121, pp. 414-422, 2007.

[27] S. Zimmermann, S. Wischhusen, and J. Müller, "Micro flame ionization detector and micro flame spectrometer," *Sensors and Actuators B: Chemical,* vol. 63, pp. 159-166, 2000.

[28] B. Alfeeli, D. Cho, M. Ashraf-Khorassani, L. T. Taylor, and M. Agah, "MEMS-based multi-inlet/outlet preconcentrator coated by inkjet printing of polymer adsorbents," *Sensors and Actuators, B: Chemical,* vol. 133, pp. 24-32, 2008.

[29] M. A. Zareian-Jahromi, M. Ashraf-Khorassani, L. T. Taylor, and M. Agah, "Design, Modeling, and Fabrication of MEMS-Based Multicapillary Gas Chromatographic Columns," *Microelectromechanical Systems, Journal of,* vol. 18, pp. 28-37, 2009.

[30] M. A. Zareian-Jahromi, M. Ashraf-Khorassani, L. T. Taylor, and M. Agah, "Design, Modeling and Fabrication of MEMS-Based Multicapillary Gas Chromatography Columns," in *North American Solid-State Sensors, Actuators, and Microsystems Workshop*, Hilton Head Island, SC, USA, 2008, pp. 256-259.

[31] M. Agah, G. R. Lambertus, R. Sacks, and K. Wise, "High-speed MEMS-based gas chromatography," *Journal of Microelectromechanical Systems,* vol. 15, pp. 1371-1378, Oct 2006.

[32] M. Agah, J. A. Potkay, G. Lambertus, R. Sacks, and K. D. Wise, "High-performance temperature-programmed microfabricated gas chromatography columns," *Journal of Microelectromechanical Systems,* vol. 14, pp. 1039-1050, 2005.

[33] M. Agah and K. D. Wise, "Low-mass PECVD oxynitride gas chromatographic columns," *Journal of Microelectromechanical Systems,* vol. 16, pp. 853-860, 2007.

[34] A. Bhushan, D. Yemane, E. B. Overton, J. Goettert, and M. C. Murphy, "Fabrication and preliminary results for LiGA fabricated nickel micro gas chromatograph columns," *Journal of Microelectromechanical Systems,* vol. 16, pp. 383-393, 2007.

[35] E. S. Kolesar, Jr. and R. R. Reston, "Review and summary of a silicon micromachined gas chromatography system," *IEEE Transactions on Components, Packaging, and Manufacturing Technology Part B: Advanced Packaging,* vol. 21, pp. 324-328, 1998.

[36] H. Noh, C. Timmons, P. J. Hesketh, and D. W. Hess, "Performance of miniature parylene gas chromatographic column," Honolulu, HI, United States, 2004, pp. 184-200.

[37] S. Reidy, D. George, M. Agah, and R. Sacks, "Temperature-Programmed GC Using Silicon Microfabricated Columns with Integrated Heaters and Temperature Sensors," *Anal. Chem.,* vol. 79, pp. 2911-2917, 2007.

[38] R. R. Reston and E. S. Kolesar, Jr., "Silicon-micromachined gas chromatography system used to separate and detect ammonia and nitrogen dioxide - Part I: Design, fabrication, and integration of the gas chromatography system," *Journal of Microelectromechanical Systems,* vol. 3, pp. 134-146, 1994.

[39] T. H. Risby and S. F. Solga, "Current status of clinical breath analysis," *Applied Physics B: Lasers and Optics,* vol. 85, pp. 421-426, 2006.

[40] G. Wiranto, M. R. Haskard, D. E. Mulcahy, D. E. Davey, and E. F. Dawes, "Microengineered open tubular columns for GC analysis," *Proceedings of SPIE - The International Society for Optical Engineering,* vol. 3891, pp. 168-177, 1999.

[41] C. M. Yu, M. Lucas, J. C. Koo, P. Stratton, T. DeLima, and E. Behymer, "A high performance hand-held gas chromatograph," Anaheim, CA, USA, 1998, pp. 481-6.

[42] A. Bhushan, D. Yemane, J. Goettert, E. B. Overton, and M. C. Murphy, "Fabrication and testing of high aspect ratio metal micro-gas chromatograph columns," Anaheim, CA, United States, 2004, pp. 321-324.

[43] S. Reidy, D. George, M. Agah, and R. Sacks, "Temperature-programmed GC using silicon microfabricated columns with integrated heaters and temperature sensors," *Analytical Chemistry,* vol. 79, pp. 2911-2917, 2007.

[44] G. Lambertus, A. Elstro, K. Sensenig, J. Potkay, M. Agah, S. Scheuering, K. Wise, F. Dorman, and R. Sacks, "Design, Fabrication, and Evaluation of Microfabricated Columns for Gas Chromatography," *Analytical Chemistry,* vol. 76, pp. 2629-2637, 2004.

[45] J. A. Potkay, J. A. Driscoll, M. Agah, R. D. Sacks, and K. D. Wise, "A high-performance microfabricated gas chromatography column," Kyoto, Japan, 2003, pp. 395-398.

[46] S. Reidy, G. Lambertus, J. Reece, and R. Sacks, "High-Performance, Static-Coated Silicon Microfabricated Columns for Gas Chromatography," *Analytical Chemistry,* vol. 78, pp. 2623-2630, 2006.

[47] M. J. E. Golay, "1ST INTERNATIONAL-SYMPOSIUM ON GLASS CAPILLARY CHROMATOGRAPHY, HINDELANG, GERMANY, MAY 4-7, 1975 - OPENING ADDRESS," *Chromatographia,* vol. 8, pp. 421-421, 1975.

[48] R. L. Grob and E. F. Barry, *Modern Practice of Gas Chrmatography* fourth ed. Hoboken, NJ: Wiey-Interscience, 2004.

[49] E. S. Glenn, "Relationships for modeling the performance of rectangular gas chromatographic columns," *Journal of Microcolumn Separations,* vol. 13, pp. 285-292, 2001.

[50] L. S. Ettre and J. V. Hinshaw, *Basic Relationships of Gas Chromatography* Advanstar Communications, 1993.

[51] J. V. Hinshaw and L. S. Ettre, *Introduction to open-Tubular Column Gas Chromatography* Advanstar Communication 1994.

[52] R. T. Ghijsen, H. Poppe, J. C. Kraak, and P. P. E. Duysters, "The Mass Loadability of Various Stationary Phases in Gas Chromatography," *chromatographia* vol. 27, p. 7, 1989.

[53] V. P. Zhdanov, V. N. Sidelnikov, and A. A. Vlasov, "Dependence of the efficiency of a multicapillary column on the liquid phase loading method," *Journal of Chromatography A,* vol. 928, pp. 201-207, 2001.

[54] A. D. Radadia, R. I. Masel, and M. A. Shannon, "New Column Designs for MicroGC," in *Solid-State Sensors, Actuators and Microsystems Conference, 2007. TRANSDUCERS 2007. International*, 2007, pp. 2011-2014.

[55] C. T. Culbertson, S. C. Jacobson, and J. M. Ramsey, "Dispersion Sources for Compact Geometries on Microchips," *Analytical Chemistry,* vol. 70, pp. 3781-3789, 1998.

[56] C. W. R. Kong, S. Fields, and M. Lee,, "Deactivation of small-diameter fused-silica capillary columns for gas and supercritical fluid chromatography," *Chromatographia,* vol. 18, pp. 362-266, 1984.

[57] T. R. Anthony, "Anodic bonding of imperfect surfaces," *Journal of Applied Physics,* vol. 54, pp. 2419-2428, 1983.

[58] M. j. Madou, *Fundamental of Microfabrication* Second ed.: CRC Press, 2002.

[59] R. M. White, *Fluid Mechanics*, 5th ed.: McGraw-Hill, 2003.

[60] P. R. Lewis, P. Manginell, D. R. Adkins, R. J. Kottenstette, D. R. Wheeler, S. S. Sokolowski, D. E. Trudell, J. E. Byrnes, M. Okandan, J. M. Bauer, R. G. Manley, and C. Frye-Mason, "Recent advancements in the gas-phase MicroChemLab," *IEEE Sensors Journal,* vol. 6, pp. 784-95, 2006.

[61] Q.-S. Qu, F. Shen, M. Shen, X.-Y. Hu, G.-J. Yang, C.-Y. Wang, C. Yan, and Y.-K. Zhang, "Open-tubular gas chromatography using capillary coated with octadecylamine-capped gold nanoparticles," *Analytica Chimica Acta,* vol. 609, pp. 76-81, 2008.

[62] G. M. Gross, J. W. Grate, and R. E. Synovec, "Development and evaluation of gold-centered monolayer protected nanoparticle stationary phases for gas chromatography," *Journal of Chromatography A,* vol. 1060, pp. 225-236, 2004.

[63] A. D. Mello, "on-chip chromatpgraphy: the last twenty years," *Lab on a Chip,* vol. 2, pp. 48-54, 2002.

[64] K. Chenoweth, S. Cheung, A. C. T. Van Duin, W. A. Goddard Iii, and E. M. Kober, "Simulations on the thermal decomposition of a poly(dimethylsiloxane) polymer using the ReaxFF reactive force field," *Journal of the American Chemical Society,* vol. 127, pp. 7192-7202, 2005.

[65] E. Vallés, C. Sarmoria, M. Villar, M. Lazzari, and O. Chiantore, "Model polydimethylsiloxanes subjected to thermal weathering: effect on molecular weight distributions," *Polymer Degradation and Stability,* vol. 69, pp. 67-71, 2000.

[66] G. M. Gross, D. A. Nelson, J. W. Grate, and R. E. Synovec, "Monolayer-protected gold nanoparticles as a stationary phase for open tubular gas chromatography," *Analytical Chemistry,* vol. 75, pp. 4558-4564, 2003.

[67] G. M. Gross, J. W. Grate, and R. E. Synovec, "Monolayer-protected gold nanoparticles as an efficient stationary phase for open tubular gas chromatography using a square capillary: Model for chip-based gas chromatography in square cornered microfabricated channels," *Journal of Chromatography A,* vol. 1029, pp. 185-192, 2004.

[68] B. Alfeeli, S. Ali, V. Jain, R. Montazami, J. Heflin, and M. Agah, "MEMS-based gas chromatography columns with nano-structured stationary phases," in *Sensors, 2008 IEEE*, 2008, pp. 728-731.

[69] M. Pumera, J. Wang, E. Grushka, and R. Polsky, "Gold nanoparticle-enhanced microchip capillary electrophoresis," *Analytical Chemistry,* vol. 73, pp. 5625-5628, 2001.

[70] M. Stadermann, A. D. McBrady, B. Dick, V. R. Reid, A. Noy, R. E. Synovec, and O. Bakajin, "Ultrafast gas chromatography on single-wall carbon nanotube stationary phases in microfabricated channels," *Analytical Chemistry,* vol. 78, pp. 5639-5644, 2006.

[71] V. R. Reid, M. Stadermann, O. Bakajin, and R. E. Synovec, "High-speed, temperature programmable gas chromatography utilizing a microfabricated chip with an improved carbon nanotube stationary phase," *Talanta,* vol. 77, pp. 1420-1425, 2009.

[72] L.-M. Yuan, C.-X. Ren, L. Li, P. Ai, Z.-H. Yan, M. Zi, and Z.-Y. Li, "Single-walled carbon nanotubes used as stationary phase in GC," *Analytical Chemistry,* vol. 78, pp. 6384-6390, 2006.

[73] T. O'Mahony, V. P. Owens, J. P. Murrihy, E. Guihen, J. D. Holmes, and J. D. Glennon, "Alkylthiol gold nanoparticles in open-tubular capillary electrochromatography," *Journal of Chromatography A,* vol. 1004, pp. 181-193, 2003.

[74] D. Wang, S. L. Chong, and A. Malik, "Sol−Gel Column Technology for Single-Step Deactivation, Coating, and Stationary-Phase Immobilization in High-Resolution Capillary Gas Chromatography," *Analytical Chemistry,* vol. 69, pp. 4566-4576, 1997.

[75] M. Schlesinger and M. Paunovic, *Modern electroplating*, Fourth ed. New York: John Wiley & Sons, inc., 2000.

[76] S. khorasani, A. Motieifar, and B. Rashadian, "Optimal Pulse shapes for periodic revere electroplating " *iranian journal of science & technology, transistion B,* vol. 27, pp. 701-707, 2003.

[77] T. Fujita, S. Nakamichi, S. Ioku, K. Maenaka, and Y. Takayama, "Seedlayer-less gold electroplating on silicon surface for MEMS applications," *Sensors and Actuators A: Physical,* vol. 135, pp. 50-57, 2007.

[78] A. Ulman, "Formation and Structure of Self-Assembled Monolayers," *Chemical Reviews,* vol. 96, pp. 1533-1554, 1996.

[79] M. D. Ventra, S. Evoy, and J. R. Heflin, *Introduction to nanoscale science and technology*. Boston: Springer Science, 2004.